

Can Diffusion Models Provide Rigorous Uncertainty Quantification for Bayesian Inverse Problems?

Evan Scope Crafts¹, Member, IEEE, and Umberto Villa¹, Member, IEEE

¹Oden Institute for Computational Engineering and Sciences, The University of Texas at Austin, Austin, TX USA 78712

Corresponding author: Umberto Villa (email: uvilla@oden.utexas.edu).

This work was supported by the National Institute of Biomedical Imaging and Bioengineering of the National Institutes of Health under award numbers R01EB031585 and R01EB034261. Code is available at: <https://doi.org/10.5281/zenodo.14908137>.

ABSTRACT

In recent years, the ascendance of diffusion modeling as a state-of-the-art generative modeling approach has spurred significant interest in their use as priors in Bayesian inverse problems. However, it is unclear how to optimally integrate a diffusion model trained on the prior distribution with a given likelihood function to obtain posterior samples. While algorithms that have been developed for this purpose can produce high-quality, diverse point estimates of the unknown parameters of interest, they are often tested on problems where the prior distribution is analytically unknown, making it difficult to assess their performance in providing rigorous uncertainty quantification. In this work, we introduce a new framework, Bayesian Inverse Problem Solvers through Diffusion Annealing (BIPSDA), for diffusion model based posterior sampling. The framework unifies several recently proposed diffusion model based posterior sampling algorithms and contains novel algorithms that can be realized through flexible combinations of design choices. Algorithms within our framework were tested on model problems with a Gaussian mixture prior and likelihood functions inspired by problems in image inpainting, x-ray tomography, and phase retrieval. In this setting, approximate ground-truth posterior samples can be obtained, enabling principled evaluation of the performance of the algorithms. The results demonstrate that BIPSDA algorithms can provide strong performance on the image inpainting and x-ray tomography based problems, while the challenging phase retrieval problem, which is difficult to sample from even when the posterior density is known, remains outside the reach of the diffusion model based samplers.

INDEX TERMS Bayesian inference, diffusion models, generative AI, optimization, machine learning, posterior probability, uncertainty quantification

I. INTRODUCTION

Inverse problems, which aim to estimate an unknown parameter of interest from observed data (measurements), provide a principled way to integrate data with existing scientific knowledge. However, many important inverse problems throughout the sciences are *ill-posed*—the measurements alone do not contain enough information to uniquely and stably estimate the parameter of interest. In the Bayesian inverse problem framework, this difficulty is addressed through the integration of prior knowledge regarding the parameter of interest, which enables both point estimation of the unknown parameter and rigorous uncertainty quantification [1], [2]. This can

facilitate risk-informed analysis and decision making, which is particularly important in the context of safety-critical systems (e.g., medical imaging [3] or earthquake detection [4] systems), where accurate risk assessments can save lives.

The Bayesian framework requires knowledge of the prior probability distribution of the unknown parameter. However, for many problems of interest (e.g., image reconstruction) the distribution of the unknown parameters has a complex structure that is not easily captured by hand-crafted prior distributions (e.g., Gaussian, total variation, or sparsity-inducing priors). Using an inaccurate prior can lead to biased point estimates of

the unknown parameter and incorrect predictions of the parameter uncertainty.

The success of generative modeling [5], [6] in capturing the structure of complex high-dimensional probability distributions in recent years has spurred considerable interest in the use of generative modeling to overcome this limitation [7]. In particular, over the last four years the rise to prominence of diffusion modeling [8]–[10] as a state-of-the-art generative modeling approach has been coupled with significant interest in their use as prior distributions in Bayesian inference. Here a common strategy is to obtain posterior samples by pretraining a diffusion model on samples from the prior distribution and integrating the pretrained model with the likelihood function (which is assumed to be known analytically) at inference time [11]–[15]. This general strategy has the advantage of enabling the same diffusion model to be used in conjunction with many different data acquisition designs without retraining, and has shown considerable promise. However, there is no consensus on how to optimally integrate the diffusion model and the likelihood function. While several algorithms have been proposed for this purpose, test-bed problems with no analytically-known ground-truth prior are often used to illustrate the performance of such methods. In this setting, the performance of the algorithms is often assessed using sample quality metrics like peak signal-to-noise ratio, as well as heuristic arguments regarding the sample diversity. This makes it difficult to assess the accuracy of these methods in capturing the global structure of the posterior.

In this paper, we introduce a unified framework, Bayesian Inverse Problem Solvers through Diffusion Annealing (BIPSDA), for solving Bayesian inverse problems with diffusion models. The framework generalizes and extends two recently proposed algorithms, Diffusion Annealing Posterior Sampling (DAPS) [16] and DiffPIR [17], for solving Bayesian inverse problems with diffusion models. These two algorithms have achieved strong performance on a number of canonical imaging reconstruction problems, including non-linear problems such as phase retrieval that were previously too difficult for diffusion model based solvers [16]. In our framework, the DAPS and DiffPIR algorithms can be recovered through specific design choices, while new algorithms can be realized through exploration of the algorithmic design space. We provide examples of several novel algorithms within our framework, including a class of approaches inspired by the randomize-then-optimize (RTO) method [18], [19] for sampling from posterior distributions.

We systematically evaluated the performance of algorithms in the proposed framework, including the DAPS and DiffPIR algorithms and the novel RTO-based algorithms, on a set of model problems. Each model problem uses a Gaussian mixture prior. This choice of prior has

two key advantages. First, under this choice the posterior density is known and approximate ground-truth posterior samples can be obtained, enabling rigorous analysis of the performance of the BIPSDA algorithms. Second, under this choice the noisy prior scores, a key component of diffusion models that is learned from data, can be formed analytically. This allows us to decompose the error in the posterior sampler into two components: error inherent to the algorithm, and error due to incorrect modeling of the prior distribution. For the likelihood functions, we considered benchmark problems inspired by classic image restoration/reconstruction problems: simple linear inpainting problems (in both low and high noise regimes), as well as nonlinear x-ray tomography and phase retrieval based problems.

In each experiment, the performance of the BIPSDA algorithms was evaluated by comparing the algorithm samples with the approximate ground-truth samples using four different metrics: the central moment discrepancy (CMD) [20], maximum mean discrepancy (MMD) [21], and the errors in both the predicted posterior mean and pointwise variance. This enables principled evaluation of the ability of various BIPSDA algorithms to capture both the local and global posterior structure.

The remainder of this paper is organized as follows. In Section II, we provide relevant background on Bayesian inverse problems and diffusion models. In Section III we introduce the proposed BIPSDA framework, discuss its relationship to previously proposed algorithms, and provide examples of algorithms that can be realized within the framework. Section IV provides details regarding the numerical studies, while results are shown in Section V. A discussion of the results and the conclusion is given in Section VI.

II. BACKGROUND

In this section, we provide relevant background on Bayesian inverse problems and diffusion models. We also provide a brief overview of a popular class of algorithms, referred to here as hijacking algorithms, for solving Bayesian inverse problems with diffusion models. This overview serves to both motivate the proposed framework and to introduce algorithmic ideas relevant to the present work.

A. BAYESIAN INVERSE PROBLEMS

In inverse problems, the relationship between the measurements $\mathbf{y} \in \mathbb{R}^K$ and the unknown variable of interest $\mathbf{m} \in \mathbb{R}^D$ is captured by the likelihood function $\pi_{\text{like}}(\mathbf{y} | \mathbf{m})$, where here and throughout the remainder of this work we assume the measurements and the unknown variable lie in finite-dimensional Euclidean spaces. Concretely, under the assumption of additive Gaussian noise, the measurements can be written as

$$\mathbf{y} = f(\mathbf{m}) + \mathbf{z}, \quad \mathbf{z} \sim \mathcal{N}(\mathbf{z}; \mathbf{0}, \Sigma_{\mathbf{z}}), \quad (1)$$

where $f : \mathbb{R}^D \rightarrow \mathbb{R}^K$ is known as the forward model, and $\Sigma_{\mathbf{z}} \in \mathbb{R}^{K \times K}$ is the covariance matrix of the noise distribution. The corresponding likelihood function is given as $\pi_{\text{like}}(\mathbf{y} | \mathbf{m}) = \mathcal{N}(\mathbf{y}; f(\mathbf{m}), \Sigma_{\mathbf{z}})$.

By Bayes' Theorem, the posterior distribution $\pi_{\text{post}}(\mathbf{m} | \mathbf{y})$ of the unknown variable is related to the likelihood function and prior density function $\pi_{\text{pr}}(\mathbf{m})$ by the following expression:

$$\pi_{\text{post}}(\mathbf{m} | \mathbf{y}) \propto \pi_{\text{like}}(\mathbf{y} | \mathbf{m}) \pi_{\text{pr}}(\mathbf{m}). \quad (2)$$

The goal of Bayesian inverse problems is to characterize the posterior distribution. In particular, depending on the application, various quantities, such as the mean, covariance, or higher-order moments of the posterior, may be of interest. While for certain choices of priors and likelihood functions (e.g., linear-Gaussian likelihood and Gaussian prior), these quantities can be computed in closed form, in general this is not tractable, and in practice Monte Carlo methods are often used to estimate the quantities of interest from samples.

B. DIFFUSION MODELS

Broadly, the goal of generative modeling can be described as follows: given a set of samples $\mathcal{M} = \{\mathbf{m}_i\}_{i=1}^{N_s}$ from a distribution of interest with density function $\pi_0(\mathbf{m})$, obtain a set of samples from $\pi_0(\mathbf{m})$ that are not in \mathcal{M} . In diffusion modeling, these samples are obtained by reversing a predefined noising process [9], [10]. This noising process can be written as a stochastic differential equation (SDE). In particular, the variance exploding (VE) form of the diffusion SDE can be written as follows [10]:

$$d\mathbf{m}(t) = \sqrt{2\dot{\sigma}(t)\sigma(t)} d\mathbf{w}(t), \quad t \in [0, T], \quad (3)$$

where $\sigma(t)$ is a predefined noise schedule, $\mathbf{w}(t)$ is the Wiener process, and $\mathbf{m}(0) \sim \pi_0(\mathbf{m})$. Under this SDE, the conditional distribution of $\mathbf{m}(t)$ given $\mathbf{m}(0)$ is given by the *noising distribution* $\pi_{t|0}(\mathbf{m}(t) | \mathbf{m}(0)) = \mathcal{N}(\mathbf{m}(t); \mathbf{m}(0), \sigma^2(t)\mathbf{I})$, where here and throughout the remainder of this work we have assumed $\sigma(0) = 0$ for simplicity. This implies that solving the forward SDE is equivalent to sampling from a Gaussian. Further, for large enough T , the distribution $\pi_T(\cdot)$ will be approximately Gaussian.

To sample from $\pi_0(\mathbf{m})$, we can first sample from the Gaussian approximation of $\pi_T(\mathbf{m}(T))$ and then reverse the noising process in (3). Here there are two main methods to reverse the noising process [10]: an SDE-based approach and an ordinary differential equation (ODE) based approach. The SDE-based approach leverages the remarkable fact [22] that (3) admits a time-reversal that matches the marginal distributions $\pi_t(\mathbf{m}(t))$. This SDE takes the following form:

$$d\mathbf{m}(t) = -2\dot{\sigma}(t)\sigma(t)\nabla_{\mathbf{m}(t)} \log \pi_t(\mathbf{m}(t)) dt + \sqrt{2\dot{\sigma}(t)\sigma(t)} d\mathbf{w}(t). \quad (4)$$

The ODE based approach is based on the fact that there exists an ODE that has the same marginal distributions $\pi_t(\mathbf{m}(t))$ as the forward and reverse SDEs. This ODE, known as the probability flow ODE, has the following form:

$$d\mathbf{m}(t) = -\dot{\sigma}(t)\sigma(t)\nabla_{\mathbf{m}(t)} \log \pi_t(\mathbf{m}(t)) dt. \quad (5)$$

As the SDE and ODE approaches have the same marginal distributions, they are equivalent in probability when the score $\nabla_{\mathbf{m}(t)} \log \pi_t(\mathbf{m}(t))$ is known. However, the sample trajectories realized by the two formulations differ, and both empirical and theoretical results have provided evidence that the SDE based approach is more robust to score approximation error [23], [24].

Both the reverse SDE and probability flow ODE depend on $\nabla_{\mathbf{m}(t)} \log \pi_t(\mathbf{m}(t))$, the score (the gradient of the log-density) of the time- t marginal distribution of $\mathbf{m}(t)$. These vector fields are *a priori* unknown but can be learned from the provided samples using a parameterized model $s_{\theta}(\mathbf{m}(t), t) : \mathbb{R}^D \times \mathbb{R}_+ \rightarrow \mathbb{R}^D$ (the *score model*) with parameters $\theta \in \mathbb{R}^P$. We use θ^* to denote the optimized parameters of the model, which are obtained by minimizing the following objective over the set of samples \mathcal{M} [10]:

$$L(\theta) = \frac{1}{2} \int_{T_{\min}}^T w(t) \sum_{i=1}^{N_s} \mathbb{E}_{\mathbf{z}} \left\| s_{\theta}(\mathbf{m}_i(t); \sigma(t)) + \frac{\mathbf{z}}{\sigma(t)} \right\|_2^2 dt. \quad (6)$$

In the above objective, which is based on the denoising score matching objective originally introduced by Vincent [25], $w(t)$ is a specified weighting function, $\mathbf{m}_i(t) = \mathbf{m}_i + \sigma(t)\mathbf{z}$ is a sample from the noising distribution $\pi_{t|0}(\mathbf{m}(t) | \mathbf{m}(0) = \mathbf{m}_i)$, \mathbf{z} is white noise, and the lower integral limit $T_{\min} \geq 0$ is needed to ensure the objective is well-conditioned.

C. HIJACKING APPROACHES

The ascendance of diffusion models as a state-of-the-art generative modeling technique has spurred significant research on their use in the context of Bayesian inverse problems. In particular, there has been substantial interest in leveraging diffusion models trained on the prior distribution of a given inverse problem to sample from the posterior distribution, i.e., setting $\pi_0 = \pi_{\text{pr}}$. This general strategy has the advantage of enabling the same diffusion model to be used to sample from many posterior distributions corresponding to different choices of likelihood function without retraining the score model. In the remainder of this section, we discuss one algorithmic framework, which we refer to as the hijacking class of approaches, that follows this general strategy.

The main idea of the hijacking approaches is as follows: Given a diffusion model for the prior distribution, replace the $\nabla_{\mathbf{m}(t)} \log \pi_t(\mathbf{m}(t))$ term in (4) with $\nabla_{\mathbf{m}(t)} \log \pi_{t|\mathbf{y}}(\mathbf{m}(t) | \mathbf{y})$ to sample from the posterior,

and expand the $\pi_{t|\mathbf{y}}(\mathbf{m}(t) | \mathbf{y})$ term using Bayes' Theorem. This yields the following reverse SDE:

$$d\mathbf{m}(t) = -2\dot{\sigma}(t)\sigma(t)\nabla_{\mathbf{m}(t)}[\log \pi_t(\mathbf{m}(t)) + \log \pi_{\mathbf{y}|t}(\mathbf{y} | \mathbf{m}(t))] dt + \sqrt{2\dot{\sigma}(t)\sigma(t)} d\mathbf{w}(t). \quad (7)$$

In the above equation, an estimate of $\nabla_{\mathbf{m}(t)} \log \pi_t(\mathbf{m}(t))$ is given by the score model of the diffusion model pre-trained on the prior distribution. The $\nabla_{\mathbf{m}(t)} \log \pi_{\mathbf{y}|t}(\mathbf{y} | \mathbf{m}(t))$ term, which is known as the *noisy likelihood function* [16], then ‘‘hijacks’’ the pre-trained diffusion process with information provided by the measurements. However, while the distribution of \mathbf{y} given $\mathbf{m}(0)$ is given by the likelihood function, the noisy likelihood function is not known. In particular, computation of the noisy likelihood function

$$\pi_{\mathbf{y}|t}(\mathbf{y} | \mathbf{m}(t)) = \int \pi_{\text{like}}(\mathbf{y} | \mathbf{m}(0)) \pi_{0|t}(\mathbf{m}(0) | \mathbf{m}(t)) d\mathbf{m}(0), \quad (8)$$

is in general intractable. In practice this issue is resolved by using simple approximations of the *denoising distribution* $\pi_{0|t}(\mathbf{m}(0) | \mathbf{m}(t))$ [14], [26]–[28]. For example, in [14], the denoising distribution is modeled as a Dirac delta with mass centered on $\mathbb{E}[\mathbf{m}(0) | \mathbf{m}(t)]$, and Tweedie’s formula [29] is employed to compute the expectation. In the approach of Boys et al [26], a Gaussian approximation is employed, with the mean and covariance of the Gaussian computed using a generalized version of Tweedie’s formula [30]. However, this approach is only applicable when the likelihood function is linear-Gaussian, as otherwise the integral in (8) cannot be straightforwardly computed.

The approaches in [14] and [26] discussed above use simple approximations of the denoising distribution to make the integral in (8) tractable and enable approximation of the noisy likelihood function. In particular, both approaches use unimodal approximations. While this may be a good approximation for many prior distributions of interest when $t \approx 0$, if the prior is multimodal then $\pi_{0|t}(\mathbf{m}(0) | \mathbf{m}(t))$ will be multimodal as well for large enough t . There can therefore be significant errors in the approximation of the noisy likelihood function for large t , which in turn induces errors in the distribution of $\mathbf{m}(t)$ in (7). These errors are difficult for subsequent hijacking iterations to correct, as discretizations of the hijacking reverse SDE use small step sizes $\Delta t > 0$ that ensure $\mathbf{m}(t - \Delta t)$ will be close to $\mathbf{m}(t)$. In practice, it has been observed [16] that this can lead to poor performance on certain inverse problems (in particular, nonlinear inverse problems), with samples obtained that are consistent with the likelihood function but lie in low-density regions with respect to the prior. These issues have motivated the development of a class of methods

that address this issue by decoupling $\mathbf{m}(t)$ and $\mathbf{m}(t - \Delta t)$, which we now introduce.

III. PROPOSED APPROACH

In this section, we introduce the proposed BIPSDA framework for solving Bayesian inverse problems using diffusion models. Unlike the hijacking approaches discussed in the previous section, our framework uses a recently introduced technique called *decoupled noise annealing* [16], [17] to avoid approximation of the noisy likelihood function and prevent samples from getting stuck in low-density regions. In what follows, we first introduce the framework, which generalizes previously introduced decoupled noise annealing approaches [16], [17] and can yield new algorithms through flexible combinations of the framework’s design choices. After discussing the relationship between our framework and previously proposed decoupled noise annealing approaches, we give examples of concrete algorithms that can be realized within our framework.

A. THE FRAMEWORK

As in other decoupled noise annealing approaches [16], [17], the proposed BIPSDA framework generates a sequence of iterates that are approximate samples from the noisy posterior distribution at a series of decreasing noise levels. Specifically, each iteration is comprised of two stages: a *prediction* stage that generates a posterior sample that is consistent with the current iterate and the measurements, and a *corruption* stage in which noise is added back to the predicted posterior sample.

Concretely, given the current iterate $\mathbf{m}(t)$ and the measurements \mathbf{y} , the goal of the prediction stage is to obtain an approximate sample $\mathbf{m}(0)$ from the *prediction distribution* $\pi_{0|t,\mathbf{y}}(\mathbf{m}(0) | \mathbf{m}(t), \mathbf{y})$. In the corruption stage, $\mathbf{m}(t - \Delta t)$ is obtained by adding noise back to $\mathbf{m}(0)$, i.e., by sampling from the Gaussian noising distribution $\pi_{t-\Delta t|0}(\mathbf{m}(t - \Delta t) | \mathbf{m}(0))$. In [16], Zhang et al prove that if $\mathbf{m}(t)$ is a sample from $\pi_{t|\mathbf{y}}(\mathbf{m}(t) | \mathbf{y})$, then this procedure yields a sample from $\pi_{t-\Delta t|\mathbf{y}}(\mathbf{m}(t - \Delta t) | \mathbf{y})$. For sufficiently large T , one can assume that $\pi_{T|\mathbf{y}}(\mathbf{m}(T) | \mathbf{y}) \approx \mathcal{N}(\mathbf{m}(T); \mathbf{0}, \sigma^2(T)\mathbf{I})$. So starting from $\mathbf{m}(T)$, the prediction and corruption steps can be iteratively applied with the timestep annealed from T down to 0 to yield a sample from the posterior distribution.

The prediction stage of the algorithm outlined above requires sampling from the prediction distribution $\pi_{0|t,\mathbf{y}}(\mathbf{m}(0) | \mathbf{m}(t), \mathbf{y})$. Using Bayes’ rule and the conditional independence of \mathbf{y} from $\mathbf{m}(t)$ given $\mathbf{m}(0)$, it holds that [16]:

$$\pi_{0|t,\mathbf{y}}(\mathbf{m}(0) | \mathbf{m}(t), \mathbf{y}) \propto \pi_{\text{like}}(\mathbf{y} | \mathbf{m}(0)) \pi_{0|t}(\mathbf{m}(0) | \mathbf{m}(t)).$$

Unfortunately, while the likelihood function is known, the denoising distribution $\pi_{0|t}(\mathbf{m}(0) | \mathbf{m}(t))$ is not and requires approximation. The prediction stage can therefore be broken down into two substages: approximation

Algorithm 1 Bayesian Inverse Problem Solvers through Diffusion Annealing (BIPSDA)

- 1: **Input:** Decreasing timesteps $[t_{N_A}, t_{N_A-1}, \dots, t_0]$, likelihood function π_{like} , noise schedule $\sigma(t)$, trained score model $s_{\theta^*}(\mathbf{m}(t), t)$
 - 2: **Output:** Approximate sample from the posterior distribution $\pi_{\text{post}}(\mathbf{m} \mid \mathbf{y})$
 - 3: Initialize $\mathbf{m}(t_{N_A}) \sim \mathcal{N}(\mathbf{m}(t_{N_A}); \mathbf{0}, \sigma^2(t_{N_A})\mathbf{I})$
 - 4: **for** $i = N_A, N_A - 1, \dots, 1$ **do**
 - 5: Compute π_{aprx} as approximation of $\pi_{0|t}$ obtained using score model
 - 6: Sample $\mathbf{m}(0) \sim \pi_{\text{like}}(\mathbf{y} \mid \mathbf{m}(0))\pi_{\text{aprx}}(\mathbf{m}(0) \mid \mathbf{m}(t_i))$
 - 7: Sample $\mathbf{m}(t_{i-1}) \sim \mathcal{N}(\mathbf{m}(t_{i-1}); \mathbf{m}(0), \sigma^2(t_{i-1})\mathbf{I})$
 - 8: **end for**
 - 9: Return $\mathbf{m}(t_0)$
-

of the denoising distribution and sampling from the prediction distribution using the approximate denoising distribution. Here it is worth noting that the hijacking approaches discussed in the previous section also require approximation of the denoising distribution, and approximations used in the hijacking setting can also be used in the BIPSDA setting (e.g., the Tweedie formula based Gaussian approximation of Boys et al [26]). However, approximations in the hijacking setting must be chosen so that the integral in (8) and the subsequent score operation in (7) can be evaluated efficiently. In our setting, there are no such restrictions. In what follows, we use $\pi_{\text{aprx}}(\mathbf{m}(0) \mid \mathbf{m}(t))$ to denote an approximation of the denoising distribution $\pi_{0|t}(\mathbf{m}(0) \mid \mathbf{m}(t))$.

In summary, the BIPSDA framework requires three steps at each iteration: approximation of the denoising distribution, sampling from the prediction distribution using the approximate denoising distribution, and corruption of the predicted sample using the Gaussian noising distribution. A full outline is provided in Algorithm 1. In what follows, we discuss previously proposed methods in the literature that fall within the BIPSDA framework, with particular attention paid to the techniques used for approximating the denoising distribution and for sampling from the approximate prediction distribution. We then give examples of novel algorithms that can be realized in our framework through different choices of the approximation distribution and sampling scheme.

B. RELATIONSHIP TO PRIOR WORK

Over the last two years, several diffusion-based Bayesian inverse problem solvers have been proposed that use decoupled noise annealing. Of these approaches, the work of Zhang et al [16] is the most closely related to the proposed BIPSDA framework. In their approach,

referred to as Decoupled Annealing Posterior Sampling (DAPS), the approximation of the denoising distribution (line 5 in Algorithm 1) takes the form of a Gaussian distribution, i.e., we have that

$$\pi_{\text{aprx}}(\mathbf{m}(0) \mid \mathbf{m}(t)) = \mathcal{N}(\mathbf{m}(0); \mathbf{m}_{\text{aprx}}, \mathbf{C}_{\text{aprx}}). \quad (9)$$

Here \mathbf{m}_{aprx} and \mathbf{C}_{aprx} are the mean and covariance, respectively, of the approximation distribution. In particular, in the DAPS approach the covariance matrix is set as $\mathbf{C}_{\text{aprx}} = \beta(t)^2\mathbf{I}$, with the noise level $\beta(t)$ chosen using heuristics. The mean of \mathbf{m}_{aprx} is set as an estimate of $\mathbb{E}_{0|t}[\mathbf{m}(0) \mid \mathbf{m}(t)]$, with the estimate obtained by solving the probability flow ODE in (5) with initial value $\mathbf{m}(t)$. Note that under a particular discretization of the probability flow ODE, this estimate corresponds with Tweedie’s formula for computing the mean and is thus exact up to error in the score model. However, in general, the probability flow ODE yields a biased estimate of the mean; see Appendix A for an analysis. To sample from the corresponding approximate prediction distribution (line 6 in Algorithm 1), the DAPS approach uses the Euler–Maruyama method for discretizing Langevin dynamics (without Metropolis adjustment).

Another approach that is closely related to the present work is the DiffPIR algorithm of Zhu et al [17]. Like the DAPS algorithm, this approach models the denoising distribution as a Gaussian, with the mean set as an estimate of the conditional mean $\mathbb{E}_{0|t}[\mathbf{m}(0) \mid \mathbf{m}(t)]$ and the covariance matrix chosen to be a scalar multiple of the identity. However, in their approach, the conditional mean is estimated using Tweedie’s formula, which, as noted above, is exact up to error in the score model. Further, the noise level of the covariance matrix is set so that $\mathbf{C}_{\text{aprx}} = \sigma^2(t)\mathbf{I}$, so unlike DAPS the covariance matrix does not depend on a user-specified hyperparameter.

While the DAPS and DiffPIR algorithms both use Gaussians to model the approximation distribution, the DiffPIR algorithm does not use Langevin dynamics to sample from the corresponding prediction distribution. Instead, inspired by plug-and-play algorithms for image restoration (see, e.g., [31]), the DiffPIR algorithm obtains a “sample” by solving the maximum a posteriori (MAP) estimation problem corresponding to the prediction distribution. While lacking theoretical guarantees, it is empirically observed that DiffPIR can produce very diverse samples (see Figure 5 in [17]). Furthermore, the approach enables the use of efficient, problem-specific MAP solvers. For example, when the measurement noise is additive Gaussian and the denoising distribution is modeled as a Gaussian, the MAP point is given by evaluation of the proximal operator corresponding to the forward model $f(\cdot)$, for which specialized algorithms are available for many classes of forward models [32].

Another difference between DiffPIR and DAPS algorithms lies in the “corruption” stage of the algorithms

(line 7 of Algorithm 1). In DAPS, as in the BIPSDA framework, the corruption stage corresponds to sampling from the Gaussian noising distribution. In DiffPIR, additional flexibility is enabled through the use of the denoising diffusion implicit models (DDIM) technique introduced by Song et al [33]. In particular, in this approach, $\mathbf{m}(t_{i-1})$ depends explicitly on both $\mathbf{m}(0)$ and $\mathbf{m}(t_i)$, with an additional hyperparameter introduced to control the weighting of the two terms. For a particular choice of this hyperparameter, the explicit dependence of $\mathbf{m}(t_{i-1})$ on $\mathbf{m}(t_i)$ disappears, and the corruption approach of DAPS and the proposed BIPSDA framework is recovered.

Other diffusion-based Bayesian inverse problem solvers that use decoupled noise annealing include those proposed in [34] and [35]. In [34], a prediction-corruption decoupled noise annealing approach, dubbed SITCOM, was proposed. As in the proposed BIPSDA framework, the corruption stage of SITCOM is implemented by sampling from the Gaussian noising distribution. However, the prediction stage differs. In BIPSDA, the prediction stage aims to sample from the prediction distribution $\pi_{0|t,\mathbf{y}}(\mathbf{m}(0) | \mathbf{m}(t), \mathbf{y})$. In the SITCOM approach, the prediction stage requires first evaluating a proximal operator to obtain a point $\mathbf{m}(t)$ that is consistent with the measurement \mathbf{y} and close to the current iterate $\mathbf{m}(t)$. Tweedie’s formula is then applied to $\mathbf{m}(t)$ to obtain the prediction $\mathbf{m}(0)$. In [35], an approach similar to the DiffPIR algorithm was proposed. Unlike DiffPIR, however, which solves for the MAP point of the prediction distribution, [35] proposes the use an iterative algorithm to maximize the likelihood function, with \mathbf{m}_{aprx} used to initialize the iterative algorithm.

C. EXAMPLE ALGORITHMS

The proposed BIPSDA framework contains many novel algorithms for solving Bayesian inverse problems with diffusion models that can be realized through different choices of the approximation distribution and sampling scheme. In the following, we discuss these design choices and provide an outline of the algorithms that will be tested in the numerical studies.

Regarding the approximation of the denoising distribution, we first note that in principle, arbitrarily complex approximations of the denoising distribution can be realized by first sampling from the denoising distribution $\pi_{0|t}(\mathbf{m}(0) | \mathbf{m}(t))$ using the reverse SDE and fitting a model to the samples. However, these approximations may be computationally prohibitive in practice, as they would require many solves of the reverse SDE and a model-fitting step at each BIPDSA iteration. We therefore restrict our focus to Gaussian approximations that do not require fitting a model to samples. In particular, we consider three different methods for setting the mean \mathbf{m}_{aprx} and covariance \mathbf{C}_{aprx} of the Gaussian approxima-

tion in (9). In the first method, which is based on the DAPS algorithm, the mean is obtained by solving the probability flow ODE, and the covariance is chosen as $\mathbf{C}_{\text{aprx}} = \beta(t)^2 \mathbf{I}$, where here we set $\beta(t) = \sigma(t)$ for simplicity. In the second method, the mean and covariance are set as in the DiffPIR algorithm, with \mathbf{m}_{aprx} obtained using Tweedie’s formula and $\mathbf{C}_{\text{aprx}} = \sigma(t)^2 \mathbf{I}$. Finally, in the third method, which is inspired by the hijacking approach of Boys et al [26], both the mean and covariance of the Gaussian distribution are set using the generalized version of Tweedie’s formula [30]. In the remainder of this paper, we refer to the three methods described above respectively as the ODE, Tweedie Uncorrelated (TU), and Tweedie Correlated (TC) methods for approximating the denoising distribution.

The BIPSDA framework also provides considerable flexibility regarding the choice of sampling scheme. As in DAPS [16], Markov chain Monte Carlo (MCMC) algorithms, such as Langevin dynamics or Hamiltonian Monte Carlo [36], can be employed. The prediction distribution can also be “sampled” by solving for the MAP point of the distribution, as in the DiffPIR algorithm [17]. Finally, in this work we also consider the use of a novel approach, inspired by the randomize-then-optimize (RTO) [18], [19], [37] algorithm, for approximate sampling from the prediction distribution. Here the key idea is to obtain an approximate sample from the prediction distribution by first adding noise to both the measurement and the denoising distribution, then solving for the MAP point of the corresponding noise-perturbed prediction distribution. Concretely, assuming a Gaussian approximation of the denoising distribution, noise is added to both the mean \mathbf{m}_{aprx} of this distribution and to the measurement \mathbf{y} in the likelihood function. The noise-perturbed mean and measurement, denoted $\mathbf{m}'_{\text{aprx}}$ and \mathbf{y}' respectively, can therefore be written as follows:

$$\begin{aligned} \mathbf{m}'_{\text{aprx}} &= \mathbf{m}_{\text{aprx}} + \mathbf{r}_1, \\ \mathbf{y}' &= \mathbf{y} + \mathbf{r}_2. \end{aligned} \quad (10)$$

Here $\mathbf{r}_1 \sim \mathcal{N}(\mathbf{r}_1; \mathbf{0}, \mathbf{C}_{\text{aprx}})$, while \mathbf{r}_2 is sampled from the measurement noise distribution, e.g., for the additive Gaussian noise model in (1), we have $\mathbf{r}_2 \sim \mathcal{N}(\mathbf{r}_2; \mathbf{0}, \mathbf{\Sigma}_{\mathbf{z}})$. This approach, like the MAP approach used in DiffPIR, has the advantage of enabling efficient MAP solvers to be employed for sampling from prediction distribution. Further, in the linear-Gaussian likelihood setting, where the corresponding prediction distribution is also Gaussian, it can be proven that this approach corresponds to exact sampling from the prediction distribution [18], [38].

IV. NUMERICAL STUDIES

The performance of diffusion model based posterior sampling algorithms is often evaluated on high-dimensional problems (e.g., imaging problems), where the prior dis-

tribution is characterized implicitly through a dataset of examples (samples). In this setting, the posterior density is analytically unknown, making it difficult to evaluate the ability of the algorithm under consideration to capture the global structure of the posterior distribution and facilitate uncertainty quantification. To address this issue, we created a suite of benchmark problems for which the prior distribution, as well as the score of the denoising distribution, is analytically known. Using these benchmark problems, which use a Gaussian mixture as the prior distribution, we can rigorously assess the performance of the algorithms in our framework, which include the popular DAPS [16] and DiffPIR [17] algorithms.

The use of a Gaussian mixture prior to test the performance of diffusion model based posterior samplers has a number of advantages. First, in this setting the posterior density function is known, and in certain cases (e.g., linear-Gaussian likelihood function, where the posterior is also a Gaussian mixture) can be straightforwardly sampled from, enabling us to investigate errors in the global structure of the samples from these algorithms. Second, under this choice $\pi_t(\mathbf{m}(t))$ is also a Gaussian mixture and the noisy prior score $\nabla_{\mathbf{m}(t)} \log \pi_t(\mathbf{m}(t))$ is known analytically. This enables the decoupling of error in the score modeling error from error inherent to the sampling algorithm under consideration in a principled manner. Third, Gaussian mixture distributions can be made arbitrarily complex through the choice of the number of modes and the covariances of each component Gaussian.

Each of the studies conducted corresponds to a different choice of likelihood function for the Bayesian inverse problem. In the first and second studies, the likelihood function was inspired by image inpainting problems. We assumed a (linear) binary sampling mask as the forward model and additive Gaussian measurement noise. In the first study a low noise regime was considered, with the noise level set so that the posterior was unimodal up to numerical precision. In the second study, a high noise regime was considered where the posterior contained distinct modes. The third study considered a nonlinear likelihood function with Poisson measurement noise inspired by problems in X-ray computed tomography (CT) [39]. Finally, the fourth study considered a problem with a nonlinear Gaussian phase retrieval forward model and Gaussian measurement noise. Phase retrieval is a difficult inverse problem often arising in optical imaging applications [40] and exhibits a complicated multi-modal posterior distribution.

In each study, we tested the performance of nine algorithms within the BIPSDA framework, with each algorithm characterized by the method used to approximate the denoising distribution and the algorithm used to sample from the prediction distribution. Additional

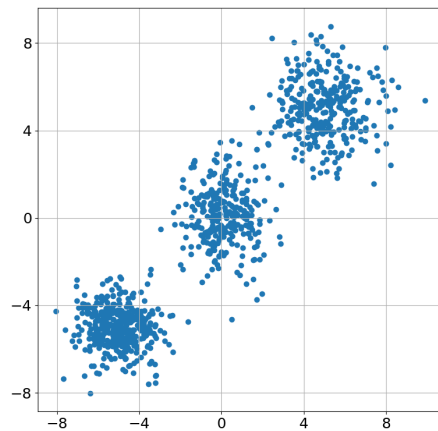


FIGURE 1. Two components of samples from the ten-dimensional Gaussian mixture prior distribution used in all of the numerical studies. The distribution has three distinct modes and each mode has a different covariance matrix.

details regarding the implementation of these algorithms, as well as the problem setting, and metrics used to evaluate the performance of the algorithms, are provided in the following subsections.

A. PROBLEM SETTINGS

As previously mentioned, all of the numerical studies described in this work consider inverse problems with inversion parameter $\mathbf{m} \in \mathbb{R}^{10}$ and a Gaussian mixture prior, i.e.,

$$\pi_{\text{pr}}(\mathbf{m}) = \sum_{i=1}^{N_m} w_i \pi_{\text{pr},i}(\mathbf{m}),$$

where each $\pi_{\text{pr},i}$ is a Gaussian, w_i is the weight of the i th component, and we set $N_m = 3$. Here $\pi_{\text{pr},1}$ has mean $[-5, \dots, -5]^T$ and identity covariance matrix, $\pi_{\text{pr},2}$ has mean $[0, \dots, 0]^T$ and a diagonal covariance matrix with entries linearly spaced between 1 and 2, and $\pi_{\text{pr},3}$ has mean $[5, \dots, 5]^T$ and a covariance matrix with the same eigenvalues as $\pi_{\text{pr},2}$ but randomly chosen eigenvectors. The corresponding weights were set as $w_1 = 0.4$, $w_2 = 0.3$, and $w_3 = 0.3$. A plot of two components of samples from this distribution is shown in Figure 1.

Both the stylized inpainting and phase retrieval studies consider likelihood functions with additive Gaussian noise, as in (1), with white noise covariance $\Sigma_{\mathbf{z}} = \tau^2 \mathbf{I}$. In the stylized inpainting studies, the forward model was given as $f(\mathbf{m}) = \mathbf{A}\mathbf{m}$, where $\mathbf{A} \in \mathbb{R}^{8 \times 10}$ is a binary subsampling operator. The noise standard deviation was set as $\tau = 0.1$ (low noise regime, $\text{SNR} \approx 30.4687$ dB) or $\tau = 5$ (high noise regime, $\text{SNR} \approx -3.5107$ dB). For the stylized phase retrieval problem, the forward model was given as $f(\mathbf{m}) = (\mathbf{B}\mathbf{m})^2$, where here the square operation is applied elementwise and $\mathbf{B} \in \mathbb{R}^{5 \times 10}$ is a matrix with i.i.d. standard Gaussian entries. The noise level for this problem was set as $\tau = 25$ ($\text{SNR} \approx -0.8243$ dB). Finally,

the likelihood function of the stylized x-ray tomography has the form

$$\pi_{\text{like}}(\mathbf{y} \mid \mathbf{m}) = \text{Poi}(f(\mathbf{m})), \quad f(\mathbf{m}) = I_0 \text{ with } \exp(-\mathbf{C}\mathbf{m}),$$

where $\text{Poi}(\cdot)$ is the Poisson distribution, the exponential operator is applied pointwise, and $\mathbf{C} \in \mathbb{R}^{15 \times 10}$. We set $I_0 = 1000$ and populated \mathbf{C} with i.i.d. random entries from the uniform distribution over the interval $[.01, .05]$ (SNR ≈ 23.1709 dB).

B. ALGORITHM IMPLEMENTATIONS

As previously discussed, in each study we analyzed the performance of nine BIPSDA algorithms, with each algorithm corresponding to a different combination of the ODE, TU, and TC methods for approximating the denoising distribution, and the Langevin dynamics (‘Lang’), MAP estimation (‘MAP’), or RTO based approaches for sampling from the corresponding prediction distribution. Throughout the remainder of this paper, we denote each of the nine BIPSDA algorithms by the name of the sampling algorithm and the name of the method for approximating the denoising distribution. For example, the BIPDA algorithm that uses Langevin dynamics to sample from the prediction distribution and the TU method to approximate the denoising distribution is denoted Lang-TU.

Each of the BIPSDA algorithms tested was implemented using $N_A = 200$ timepoints in the noise annealing, with the t_i set by polynomial interpolation between T and 0. The ODE method for approximating the denoising distribution was implemented by solving the probability flow ODE using the Euler discretization with five discretization time-steps. The above settings are the same as used by Zhang et al; see [16] for details.

The implementation of the Langevin dynamics based sampler and the MAP solver used in the MAP and RTO-based approaches was problem specific. The sampler for the stylized inpainting problem was implemented with step size $= 5 \times 10^{-5}$, 100 subiterations per algorithm iteration, and no Metropolis correction, as in [16]. The implementation was the same for the stylized x-ray tomography based problem, but with 1000 subiterations instead of 100. For the phase retrieval problem, we observed severe stability issues with unadjusted Langevin dynamics, and instead implemented Langevin dynamics with Metropolis adjustment and preconditioning [41]. Here 1000 subiterations were used with step size $= .2$, and at each iteration we fixed the preconditioning matrix as the average of a set of matrices, where each matrix in the set is the Gauss-Newton Hessian approximation [42] evaluated at different representative sample points. Regarding the MAP solver used in the MAP and RTO-based approaches, for the stylized inpainting problem we exploited the fact that the MAP point has a closed-form expression to compute the

MAP point exactly. For the stylized x-ray tomography and phase retrieval problems, we estimated the MAP point using the PyTorch implementation of the limited-memory Broyden–Fletcher–Goldfarb–Shanno (L-BFGS) algorithm [42] (40 subiterations per algorithm iteration, strong Wolfe line search).

Each of the algorithms described above was implemented using the same pretrained score model corresponding to a diffusion model with $\sigma(t) = t$ and $T = 10$. The score model was given as $s_{\theta}(\mathbf{m}(t), t) = \nabla_{\mathbf{m}(t)} g_{\theta}(\mathbf{m}(t), t)$ where $g_{\theta}(\mathbf{m}(t), t) : \mathbb{R}^{10} \times \mathbb{R}_+ \rightarrow \mathbb{R}$ was a deep neural network. In particular, the network architecture had six total hidden layers (width = 512), with the noise level $\sigma(t)$ appended to the input $\mathbf{m}(t)$ and to the network state after the 4th layer, width = 512. The network weights were trained to minimize the loss function in (6), with $N = 80,000$ total samples in the training set, $w(t) = \sigma^2(t)$, and $T_{\min} = .01$. The Adam optimizer [43] was used with learning rate 10^{-5} and a batch size of 8000 $\{\mathbf{m}_i, \mathbf{z}_i, t_i\}$ pairs (with the \mathbf{z}_i and t_i picked i.i.d. at each iteration). The network was trained for 50,000 optimization iterations. Additionally, each algorithm was also tested with the exact ground truth score $\nabla_{\mathbf{m}(t)} \log \pi_t \mathbf{m}(t)$ used instead of the score model to isolate the effect of the score modeling error from other sources of error in the algorithms’ performance.

C. EVALUATION METHODS

We evaluated the performance of the BIPSDA algorithms by comparing the samples obtained by the algorithms with those produced by a reference method (exact sampling in the linear inverse problem case, MCMC for the non-linear inverse problems). In particular, in the stylized inpainting studies, we leveraged the fact that the ground truth posterior is a Gaussian mixture to obtain exact samples from the posterior as a reference. In the stylized x-ray tomography and phase retrieval studies, we used the PyDream implementation [44] of the MT-DREAM (ZS) algorithm [45], a state-of-the-art MCMC posterior sampling algorithm for Bayesian inverse problems where the prior density function is known analytically, to obtain approximate ground truth samples from the posterior. In the stylized x-ray tomography study, we implemented PyDream with 10 chains and 200,000 iterations per chain, and obtained the final posterior samples by discarding the first half of each chain as burn-in and randomly sub-sampling the remaining samples. A similar procedure was followed in the stylized phase retrieval study, but with additional features incorporated to address the challenging nature of the problem. In particular, we took advantage of the

fact that the posterior is a mixture distribution, i.e.,

$$\begin{aligned}\pi_{\text{post}}(\mathbf{m} | \mathbf{y}) &\propto \pi_{\text{like}}(\mathbf{y} | \mathbf{m}) \pi_{\text{pr}}(\mathbf{m}) \\ &= \sum_{i=1}^{N_m} w_i \pi_{\text{like}}(\mathbf{y} | \mathbf{m}) \pi_{\text{pr},i}(\mathbf{m})\end{aligned}$$

and sampled each of the N_m components separately. For each component, we implemented PyDream with 40 chains, 200,000 iterations run per chain, and Latin hypercube sampling [46] to seed the sampling history. After discarding the first half of each chain as burn-in, the remaining samples were sub-sampled according to the weights of each of the N_m components.

The reference samples were compared to the samples produced by the BIPSDA algorithms both qualitatively and quantitatively. In particular, in each study we compared the performance of the BIPSDA algorithms to the reference over 100 total trials, with each trial corresponding to sampling from the posterior distribution $\pi_{\text{post}}(\mathbf{m} | \mathbf{y}_i)$ and \mathbf{y}_i ($i = 1, \dots, 100$) chosen i.i.d. from the measurement distribution. In each trial, 10,000 posterior samples were obtained from both the reference and each of the proposed algorithms.

For the quantitative tests, four different error metrics were used: the central moment discrepancy (CMD) metric [20], the maximum mean discrepancy (MMD) metric [21], and the two-norm error in both the predicted posterior mean and the predicted posterior pointwise variance. The CMD metric is the weighted sum of discrepancies between the central moments of the two distributions. In particular, for two distributions π_1 and π_2 , the CMD metric can be written as follows:

$$\begin{aligned}\text{CMD}(\pi_1, \pi_2) &= \frac{1}{\alpha} \|\mathbb{E}_{\pi_1}[\mathbf{m}] - \mathbb{E}_{\pi_2}[\mathbf{m}]\|_2 \\ &\quad + \sum_{k=2}^{\infty} \frac{1}{\alpha^k} \|c_k(\pi_1) - c_k(\pi_2)\|_2,\end{aligned}$$

where $c_k(\cdot)$ is the k th central moment of the given distribution and $\alpha > 0$ is a decay rate parameter. In practice, the infinite sum is truncated at some finite index K (we use $K = 5$ in this work) for computability, which is theoretically justified by the fact that the terms in the sum can be shown to converge to zero as $k \rightarrow \infty$ for large enough α . The expectations and central moments are also replaced by empirical approximations. Finally, in this work we set the decay rate as $\alpha = 4\hat{\eta}_{\text{max}}$, where $\hat{\eta}_{\text{max}}$ is an empirical estimate of

$$\eta_{\text{max}} = \mathbb{E}_{\mathbf{y}} [\|\boldsymbol{\eta}(\mathbf{y})\|_{\infty}]$$

and $\boldsymbol{\eta}(\mathbf{y}) \in \mathbb{R}^D$ is the componentwise standard deviation of the posterior distribution $\pi_{\text{post}}(\mathbf{m} | \mathbf{y})$.

The MMD metric is based on the difference between the two probability distributions in a reproducing kernel Hilbert space (RKHS) [21]. Here we chose the kernel $k(\cdot, \cdot)$ in the metric to be the sum of Gaussian radial

basis functions with different bandwidths, i.e.,

$$k(\mathbf{m}_1, \mathbf{m}_2) = \sum_{i=1}^{N_b} \exp\left(-\frac{\|\mathbf{m}_1 - \mathbf{m}_2\|_2^2}{\epsilon_i}\right),$$

with $N_b = 5$, $\epsilon_i = \bar{\epsilon} 2^{i - \lceil N_b/2 \rceil}$, and $\bar{\epsilon}$ set as the average squared two-norm distance between samples from the reference distribution (as in [21]).

V. RESULTS

In this section, representative results from the stylized inpainting, x-ray, and phase retrieval studies are shown to illustrate the performance of the proposed framework.

A. STYLIZED INPAINTING STUDIES

We first examine the performance of the framework in the stylized inpainting studies. Table 1 shows the average error in the low noise regime with regards to the mean and pointwise variance of the posterior, as well as CMD and MMD metrics, for the nine BIPSDA algorithms tested. The corresponding results in the high noise regime are given in Table 2. Here we first note that when the analytic scores are used, the Tweedie-Correlated (TC) based approaches perform comparably with the Tweedie-Uncorrelated (TU) based approaches. However, TC-based approaches were not implemented when using the learned scores, as the Jacobian of the learned score is not a reliable estimator of the denoising distribution covariance matrix. The performance of the TC-based methods in the learned score regime was thus omitted from this and all subsequent studies.

All of the methods that were tested perform fairly well in the low noise regime using the learned score, with the RTO-TU approach providing particularly strong performance. Interestingly, the Lang-ODE approach outperforms Lang-TU despite using a biased estimate of the mean of the denoising distribution (see Appendix A). In contrast, in the high noise regime, the Langevin dynamics-based approaches all perform significantly worse than the other approaches, while the MAP estimation-based approaches perform well despite lacking the theoretical basis of the Langevin dynamics and RTO-based approaches. Further, this discrepancy is not due to score modeling error, as the Langevin dynamics-based approaches perform poorly even when the analytic scores are used.

Figure 2, which displays scatter plots of samples from three different BIPSDA methods in a representative high-noise trial, provides insight into the failure of the Langevin-based approaches. In particular, it can be seen that the Langevin dynamics based approach produces samples in low-density regions with respect to the likelihood and therefore overestimates the variance of the posterior distribution. The RTO-based approach, while still overestimating the posterior variance, is much more accurate. Finally, the MAP estimation-based approach,

	Analytic Score				Learned Score			
	Mean	Variance	CMD	MMD	Mean	Variance	CMD	MMD
Lang-TU	0.029 (0.011, 0.055)	0.64 (0.44, 0.86)	0.04 (0.03, 0.06)	0.043 (0.033, 0.054)	0.046 (0.013, 0.092)	0.64 (0.43, 0.87)	0.05 (0.03, 0.07)	0.043 (0.032, 0.055)
Lang-TC	0.024 (0.009, 0.048)	0.64 (0.43, 0.87)	0.04 (0.03, 0.06)	0.043 (0.033, 0.052)	--	--	--	--
Lang-ODE	0.032 (0.016, 0.060)	0.10 (0.02, 0.21)	0.01 (0.01, 0.02)	0.002 (0.001, 0.003)	0.047 (0.016, 0.090)	0.11 (0.02, 0.25)	0.02 (0.01, 0.03)	0.002 (0.001, 0.005)
MAP-TU	0.018 (0.007, 0.031)	0.95 (0.71, 1.19)	0.06 (0.04, 0.08)	0.142 (0.135, 0.149)	0.046 (0.013, 0.093)	0.95 (0.70, 1.21)	0.07 (0.04, 0.09)	0.143 (0.133, 0.155)
MAP-TC	0.018 (0.007, 0.030)	0.96 (0.71, 1.20)	0.06 (0.04, 0.08)	0.143 (0.135, 0.151)	--	--	--	--
MAP-ODE	0.023 (0.013, 0.037)	0.47 (0.34, 0.61)	0.03 (0.02, 0.04)	0.028 (0.025, 0.032)	0.047 (0.016, 0.090)	0.47 (0.33, 0.64)	0.04 (0.02, 0.06)	0.029 (0.025, 0.035)
RTO-TU	0.022 (0.008, 0.037)	0.05 (0.02, 0.07)	0.01 (0.01, 0.01)	0.001 (0.000, 0.001)	0.044 (0.011, 0.089)	0.06 (0.02, 0.09)	0.01 (0.01, 0.02)	0.001 (0.001, 0.003)
RTO-TC	0.020 (0.008, 0.031)	0.03 (0.01, 0.06)	0.01 (0.00, 0.01)	0.001 (0.000, 0.001)	--	--	--	--
RTO-ODE	0.027 (0.013, 0.044)	1.05 (0.79, 1.28)	0.08 (0.05, 0.10)	0.051 (0.047, 0.056)	0.046 (0.016, 0.090)	1.01 (0.80, 1.22)	0.08 (0.06, 0.10)	0.050 (0.043, 0.057)
Reference	0.020 (0.009, 0.034)	0.03 (0.01, 0.07)	0.01 (0.00, 0.01)	0.001 (0.000, 0.001)	0.020 (0.009, 0.034)	0.03 (0.01, 0.07)	0.01 (0.00, 0.01)	0.001 (0.000, 0.001)

TABLE 1. Stylized inpainting study, low noise regime: Average errors in estimation of the mean and pointwise variance of the posterior distribution, and average central moment discrepancy (CMD) and maximum mean discrepancy (MMD) errors, for different BIPSDA methods (with both learned and analytic score). Interdecile ranges are also displayed in parentheses, and a reference that shows the average errors between two sets of i.i.d. samples from the ground truth posterior is included. The best-performing method with respect to each error measure is bolded. In the learned score case, with the exception of the Tweedie-Correlated (TC) approaches that were not implemented, all approaches performed well, with the MAP and RTO based approaches providing particularly strong performance.

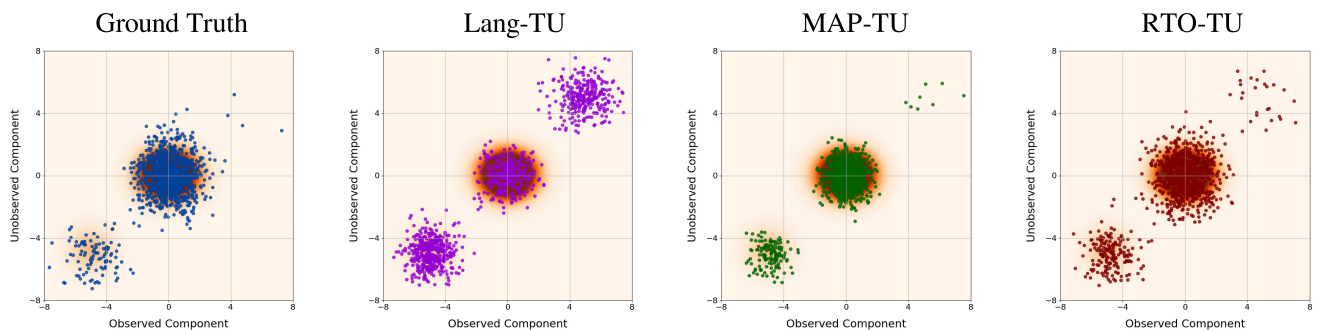


FIGURE 2. Stylized inpainting study, high noise regime: Scatter plots of samples from three different BIPSDA methods, as well as ground truth posterior samples, in a representative trial. Two components of the ten-dimensional samples are visualized, with one of the two components in the null space of the forward operator. The samples are overlaid over the posterior density. As can be seen, the RTO and MAP estimation based approaches both provide competitive performance, whereas the Langevin dynamics based approach significantly overestimates the posterior variance.

	Analytic Score				Learned Score			
	Mean	Variance	CMD	MMD	Mean	Variance	CMD	MMD
Lang-TU	10.594 (1.918, 17.898)	44.17 (33.88, 50.87)	3.14 (1.93, 4.27)	0.389 (0.188, 0.589)	10.076 (1.613, 17.952)	43.99 (33.20, 51.19)	3.05 (1.93, 4.26)	0.380 (0.145, 0.585)
Lang-TC	10.597 (2.358, 18.025)	44.84 (35.84, 51.02)	3.13 (2.06, 4.28)	0.399 (0.241, 0.593)	--	--	--	--
Lang-ODE	10.622 (2.201, 17.217)	46.76 (36.76, 53.64)	3.19 (1.98, 4.24)	0.371 (0.188, 0.506)	10.071 (1.465, 17.538)	45.76 (34.98, 53.04)	3.09 (1.98, 4.26)	0.362 (0.157, 0.514)
MAP-TU	0.246 (0.059, 0.492)	1.29 (0.55, 2.05)	0.08 (0.04, 0.13)	0.130 (0.088, 0.168)	0.262 (0.073, 0.569)	1.41 (0.61, 2.21)	0.08 (0.04, 0.13)	0.128 (0.085, 0.166)
MAP-TC	0.261 (0.054, 0.664)	1.51 (0.52, 2.61)	0.09 (0.04, 0.17)	0.133 (0.091, 0.164)	--	--	--	--
MAP-ODE	0.502 (0.307, 0.719)	0.80 (0.34, 1.38)	0.10 (0.06, 0.15)	0.035 (0.022, 0.047)	0.479 (0.324, 0.651)	0.99 (0.48, 1.93)	0.10 (0.06, 0.16)	0.035 (0.023, 0.047)
RTO-TU	1.156 (0.270, 2.140)	5.04 (1.20, 8.42)	0.34 (0.12, 0.52)	0.016 (0.002, 0.032)	1.017 (0.198, 2.087)	4.05 (0.60, 7.28)	0.29 (0.09, 0.46)	0.013 (0.002, 0.031)
RTO-TC	0.857 (0.222, 1.922)	4.72 (0.86, 12.46)	0.30 (0.09, 0.56)	0.015 (0.001, 0.043)	--	--	--	--
RTO-ODE	1.200 (0.490, 2.060)	6.24 (2.57, 9.53)	0.38 (0.19, 0.56)	0.074 (0.046, 0.107)	1.061 (0.355, 2.230)	5.10 (1.91, 7.99)	0.32 (0.14, 0.50)	0.067 (0.037, 0.096)
Reference	0.068 (0.036, 0.114)	0.22 (0.07, 0.39)	0.02 (0.01, 0.03)	0.001 (0.001, 0.001)	0.068 (0.036, 0.114)	0.22 (0.07, 0.39)	0.02 (0.01, 0.03)	0.001 (0.001, 0.001)

TABLE 2. Stylized inpainting study, high noise regime: Average errors in estimation of the mean and pointwise variance of the posterior distribution, and average central moment discrepancy (CMD) and maximum mean discrepancy (MMD) errors, for different BIPSDA methods. Interdecile ranges are also displayed in parentheses. A reference that shows the average errors between two sets of i.i.d. samples from the ground truth posterior is also included. As can be seen, the Langevin dynamics based approaches lead to poor estimates of the mean and variance of the posterior, while the MAP and RTO based approaches provide relatively strong performance.

while underestimating the variance of each of the modes, provides the most accurate estimate of the weights of the modes of all the methods tested.

B. STYLIZED X-RAY TOMOGRAPHY STUDY

We now analyze the results from the stylized x-ray tomography study. Table 3 reports the average mean, variance, CMD, and MMD errors for the different BIPSDA algorithms in this problem setting. As can be seen, in this problem setting all of the approaches we considered performed fairly well, despite the non-linearity of the forward model. The RTO-TU approach provides particularly strong performance and is the top performing approach with respect to all metrics we considered in the learned score regime. This demonstrates the potential of the RTO based approaches in the context of non-linear inverse problems.

Figure 3 shows scatter plots of samples from the ground truth posterior and the Lang-TU, MAP-TU, and RTO-TU algorithms for a representative trial. As can be seen, for this problem the posterior is approximately unimodal. Further, while all of the tested algorithms perform fairly well, the MAP-TU approach underesti-

mates the posterior variance, which is consistent with the results of the stylized inpainting study. The RTO-TU approach is able to correct the variance underestimation of the MAP-TU approach and performs similarly to the Lang-TU method on this trial.

C. STYLIZED PHASE RETRIEVAL STUDY

We now examine the performance of the algorithms in the stylized phase retrieval study. Figure 4 shows scatter plots of samples from the ground-truth posterior and the Lang-TU, MAP-TU, and RTO-TU algorithms in a representative trial (with learned score). As can be seen, both the Lang-TU and RTO-TU algorithms produce samples that lie in a low-density region between the two posterior modes. The MAP-TU approach avoids this issue, but suffers from significant underestimation of the variance of each of the modes.

Table 4 shows the average errors in estimation of the mean and variance, as well as average CMD and MMD errors, for all nine BIPSDA methods tested. Here we first note that, when the score is known analytically, the TC based approaches perform better than the TU and ODE based approaches, and on some trials produce strong

	Analytic Score				Learned Score			
	Mean	Variance	CMD	MMD	Mean	Variance	CMD	MMD
Lang-TU	0.44 (0.27, 0.64)	0.22 (0.04, 0.58)	0.12 (0.07, 0.18)	0.016 (0.008, 0.025)	0.44 (0.26, 0.68)	0.25 (0.05, 0.61)	0.12 (0.07, 0.19)	0.017 (0.009, 0.026)
Lang-TC	0.45 (0.28, 0.65)	0.23 (0.04, 0.60)	0.12 (0.08, 0.18)	0.017 (0.008, 0.028)	--	--	--	--
Lang-ODE	0.26 (0.10, 0.48)	1.19 (0.82, 1.57)	0.15 (0.08, 0.23)	0.031 (0.026, 0.036)	0.27 (0.10, 0.51)	1.14 (0.82, 1.43)	0.15 (0.08, 0.22)	0.031 (0.024, 0.037)
MAP-TU	0.12 (0.06, 0.25)	1.66 (1.07, 2.20)	0.14 (0.08, 0.21)	0.162 (0.151, 0.174)	0.13 (0.06, 0.25)	1.67 (1.06, 2.24)	0.14 (0.08, 0.21)	0.163 (0.149, 0.175)
MAP-TC	0.09 (0.03, 0.26)	1.65 (1.06, 2.20)	0.13 (0.07, 0.22)	0.160 (0.149, 0.171)	--	--	--	--
MAP-ODE	0.55 (0.35, 0.75)	0.98 (0.67, 1.26)	0.19 (0.14, 0.25)	0.075 (0.043, 0.112)	0.54 (0.35, 0.70)	1.01 (0.67, 1.33)	0.19 (0.15, 0.25)	0.076 (0.045, 0.113)
RTO-TU	0.12 (0.05, 0.27)	0.19 (0.04, 0.58)	0.04 (0.02, 0.11)	0.003 (0.001, 0.007)	0.13 (0.05, 0.26)	0.19 (0.04, 0.55)	0.04 (0.02, 0.10)	0.003 (0.001, 0.006)
RTO-TC	0.09 (0.03, 0.27)	0.18 (0.04, 0.58)	0.04 (0.01, 0.11)	0.002 (0.001, 0.007)	--	--	--	--
RTO-ODE	0.55 (0.36, 0.73)	1.51 (0.85, 2.25)	0.24 (0.16, 0.33)	0.054 (0.043, 0.068)	0.52 (0.34, 0.69)	1.41 (0.84, 2.00)	0.23 (0.16, 0.30)	0.051 (0.038, 0.069)
Reference	0.05 (0.04, 0.07)	0.07 (0.04, 0.11)	0.02 (0.01, 0.03)	0.001 (0.001, 0.001)	0.05 (0.04, 0.07)	0.07 (0.04, 0.11)	0.02 (0.01, 0.03)	0.001 (0.001, 0.001)

TABLE 3. Stylized x-ray tomography study: Average errors in estimation of the mean and pointwise variance of the posterior distribution, and average central moment discrepancy (CMD) and maximum mean discrepancy (MMD) errors, for different BIPSDA methods. Interdecile ranges are also displayed in parentheses. A reference that shows the average errors between two sets of i.i.d. samples from the ground truth posterior is also included. While all methods provide competitive performance, the RTO-TU approach outperforms all other approaches in almost every metric.

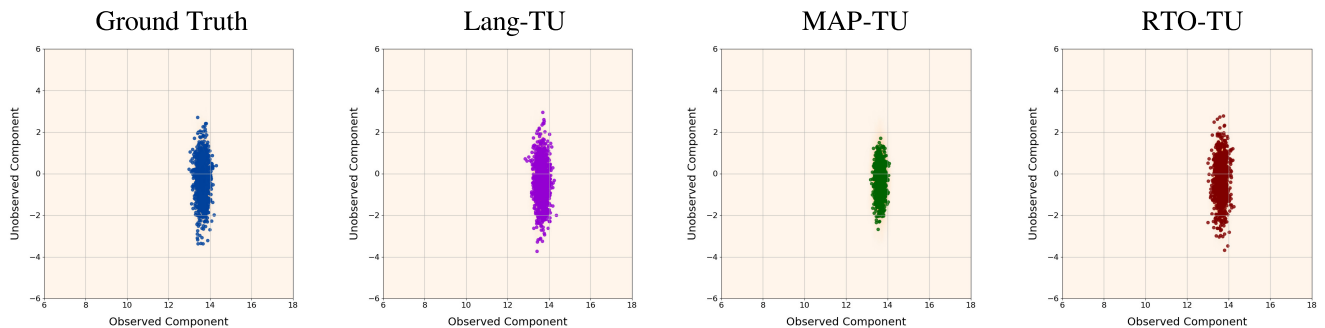


FIGURE 3. Stylized x-ray tomography study: Scatter plots of samples from three different BIPSDA methods, as well as ground truth posterior samples, in a representative trial. Here the samples have been projected onto the space spanned by the two right singular vectors corresponding to the largest and smallest singular values of the forward operator C . The samples are overlaid over a kernel density approximation of the pushforward of the posterior density under this projection. As can be seen, all three methods perform well in this setting, with the Langevin dynamics and RTO based approaches providing particularly strong performance.

	Analytic Score				Learned Score			
	Mean	Variance	CMD	MMD	Mean	Variance	CMD	MMD
Lang-TU	2.42 (0.08, 5.88)	6.26 (1.62, 14.25)	0.20 (0.01, 0.46)	0.076 (0.002, 0.152)	2.45 (0.07, 5.93)	5.73 (0.67, 14.61)	0.20 (0.01, 0.46)	0.073 (0.001, 0.157)
Lang-TC	1.90 (0.05, 4.34)	4.01 (0.13, 9.69)	0.15 (0.00, 0.34)	0.048 (0.001, 0.064)	--	--	--	--
Lang-ODE	2.53 (0.11, 5.95)	8.33 (3.60, 15.93)	0.21 (0.02, 0.47)	0.134 (0.049, 0.230)	2.54 (0.08, 5.92)	7.85 (2.47, 16.20)	0.21 (0.01, 0.47)	0.128 (0.044, 0.217)
MAP-TU	1.97 (0.06, 4.37)	5.88 (1.41, 11.63)	0.16 (0.01, 0.35)	0.129 (0.064, 0.177)	1.97 (0.08, 4.42)	5.63 (1.32, 11.46)	0.16 (0.01, 0.36)	0.127 (0.064, 0.169)
MAP-TC	1.99 (0.04, 4.74)	4.82 (1.41, 10.29)	0.16 (0.01, 0.38)	0.129 (0.072, 0.150)	--	--	--	--
MAP-ODE	2.05 (0.07, 4.72)	6.55 (2.09, 13.57)	0.17 (0.02, 0.38)	0.069 (0.015, 0.101)	2.06 (0.08, 4.75)	6.24 (1.54, 12.68)	0.17 (0.01, 0.38)	0.070 (0.015, 0.103)
RTO-TU	2.53 (0.11, 6.12)	6.83 (2.44, 13.11)	0.21 (0.02, 0.47)	0.069 (0.006, 0.165)	2.53 (0.09, 6.11)	5.98 (1.59, 12.47)	0.20 (0.01, 0.47)	0.065 (0.003, 0.156)
RTO-TC	2.04 (0.05, 4.85)	4.68 (0.20, 11.29)	0.16 (0.00, 0.37)	0.047 (0.001, 0.090)	--	--	--	--
RTO-ODE	2.57 (0.16, 5.94)	8.64 (4.03, 14.63)	0.22 (0.03, 0.47)	0.124 (0.055, 0.210)	2.58 (0.12, 5.99)	7.71 (3.15, 13.69)	0.21 (0.02, 0.47)	0.117 (0.048, 0.207)
Reference	0.24 (0.05, 0.50)	0.79 (0.08, 1.15)	0.02 (0.00, 0.04)	0.002 (0.001, 0.002)	0.24 (0.05, 0.50)	0.79 (0.08, 1.15)	0.02 (0.00, 0.04)	0.002 (0.001, 0.002)

TABLE 4. Stylized phase retrieval study: Average errors in estimation of the mean and pointwise variance of the posterior distribution, and average central moment discrepancy (CMD) and maximum mean discrepancy (MMD) errors, for different BIPSDA methods. Interdecile ranges are also displayed in parentheses, and a reference that shows the average errors between two sets of i.i.d. samples from the ground truth posterior is included. Note that for the Lang-TU and RTO-TU methods in the learned score regime, 29 and 185 samples, respectively, of the million total samples generated across the hundred trials numerically diverged and were discarded. As can be seen, all of the algorithms we analyzed produce significant errors in posterior sampling on this challenging problem.

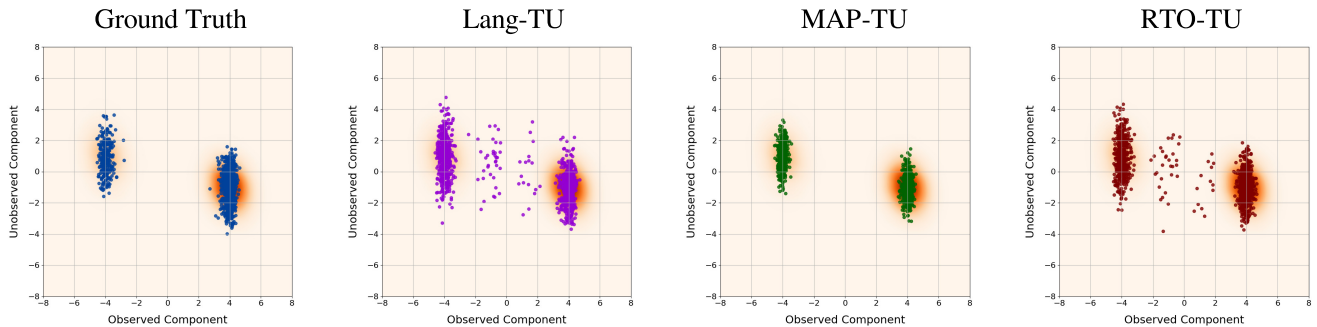


FIGURE 4. Stylized phase retrieval study: Scatter plots of samples from three different BIPSDA methods, as well as ground truth posterior samples, in a representative trial. Here the samples have been projected onto onto the space spanned by the two right singular vectors corresponding to the largest and smallest singular values of the forward operator B . The samples are overlaid over a kernel density approximation of the pushforward of the posterior density under this projection. As can be seen, the RTO and Langevin based approaches both abandon samples between the two distribution modes, while the MAP approach underestimates the variance of the modes.

performance, as evidenced by the provided interdecile ranges. This indicates that the TC approaches have some promise if a reliable approximation of the second-order score can be estimated using, e.g. the methods in [30]. However, there is wide variance in performance across the trials, and in general the TC approaches cannot fully overcome the issues observed with the TU approaches in Figure 2. All of the BIPDSA algorithms we tested thus face performance issues in this problem context.

VI. DISCUSSION AND CONCLUSION

Diffusion annealing based inverse problem solvers is an emerging class of algorithms for solving Bayesian inverse problems using a diffusion model trained on the prior distribution. In this work, we introduced a general framework, Bayesian Inverse Problem Solvers through Diffusion Annealing (BIPDSA), for this class of algorithms. This framework has two key design choices—the denoising distribution approximation and the sampler for the prediction distribution—that can be “mixed and matched” in a flexible manner. The large algorithmic design space of BIPDSA includes the previously introduced DAPS [16] and DiffPIR [17] algorithms, which have both achieved state-of-the-art performance on different image reconstruction problems.

We analyzed the performance of nine algorithms within the framework, including the DAPS algorithm, DiffPIR algorithm, and seven novel algorithms, on a suite of model problems where the posterior density is known. Here the novel algorithms were realized through combinations of ideas from DAPS and DiffPIR. We also incorporated the Tweedie Correlated (TC) technique [30] for modeling the denoising distribution and a randomize-then-optimize (RTO) technique [18], [19], [37] for fast, approximate sampling from the prediction distribution. The TC technique was previously introduced in the context of the hijacking class of diffusion-based Bayesian inverse problem solvers [26], but has not been employed in the diffusion annealing context. The RTO-based idea, to the best of the author’s knowledge, has not previously been employed in the context of diffusion modeling.

A. RESULTS ANALYSIS

The results provide insights into both the impact of specific design choices with our framework and the performance of diffusion model based inverse problem solvers generally. Regarding the choice of denoising distribution approximation, we note that approaches that use the TC technique provide the best performance on the two non-linear inverse problems we tested when the prior score is assumed to be known analytically. However, in our implementation this technique is currently only applicable when the score is known exactly. The training of an auxiliary neural network model to approximate higher-order moments of the data distribution is required

in the learned score setting [30]. It is also worth noting that in general, the TU technique, which uses an unbiased estimator of the mean of the denoising distribution, performs better than the ODE technique, which uses a biased estimate.

Regarding the sampler for the prediction distribution, the results demonstrate that the MAP estimation based approaches, despite lacking firm theoretical foundations, perform well in recovering the global structure of the posterior distribution. However, they systematically underestimate the variance of each of the posterior modes, which is unsurprising given that the MAP approaches do not actually sample from the prediction distribution. The RTO technique, which is equivalent to exact sampling from the prediction distribution when the likelihood function is linear-Gaussian [38], partially resolves this issue and provides better performance than the MAP based approaches on the stylized x-ray tomography problem and inpainting problems. Finally, the Langevin dynamics based approaches work well when the posterior is unimodal (low noise regime of the stylized inpainting problem and stylized x-ray tomography problem). However, in the case of multimodal posteriors (as in the high noise regime of the stylized inpainting problem), Langevin dynamics struggles to properly incorporate the measurement information. Further, on the phase retrieval problem, Langevin dynamics without Metropolis correction completely fails, and the incorporation of a Metropolis adjustment and preconditioning was required to obtain competitive performance.

Overall, the results demonstrate that the BIPDSA framework can provide strong performance on problems with unimodal posterior distributions. Strong performance is also attainable on problems that have multimodal posteriors and linear forward models, although in this setting the performance of the framework is sensitive to the algorithmic design choices made. On the stylized phase retrieval problem, however, all of the BIPDSA algorithms we tested produced inaccurate uncertainty estimates. This is reflective of the extremely challenging nature of the problem, for which even conventional MCMC algorithms that require knowledge of the posterior density struggle to perform well.

B. LIMITATIONS AND FUTURE DIRECTIONS

The proposed benchmark problems provide useful insight on the ability of diffusion annealing based inverse problem solvers to provide rigorous estimates of the uncertainty of the posterior distribution. While results are promising, there are a few limitations of the present work that require further investigation.

First, it is of interest to develop an extension of TC technique to the case in which the score is not known analytically but is learned from data. This could potentially be accomplished through regularization of

the TC estimator and the use of an additional neural network trained to match the second-order moments of the data distribution [30]. Second, the algorithms in our framework were tested on stylized model problems that enable principled performance analysis but have low dimensionality. While previously established algorithms within our framework have been shown to produce high quality samples for large-scale problems (including image reconstruction), it is of interest to systematically evaluate the performance BIPSDA framework in these high-dimensional settings.

It is also of interest to improve the performance of BIPSDA algorithms on challenging non-linear problems like phase retrieval. Here we first note that in this study there were cases where posterior samples numerically diverged due to large error in the learned score in low probability regions of the prior. This could potentially be addressed through the incorporation of second-order score model derivative information into the score training, which has been shown to improve model accuracy in low-density regions in other problem contexts [47]. Further, even with the score known analytically, the BIPSDA algorithms performed poorly on some of the trials, and additional algorithmic innovations are required to address this. In particular, it is of interest to explore modifications to the proposed RTO technique, such as apodizing the RTO noise perturbation in early BIPSDA iterations or metropolizing the RTO sampling, to improve performance on challenging problems like this one.

Appendix A

MEAN ESTIMATION WITH PROBABILITY FLOW ODES

In this appendix, we analyze the relationship between the Tweedie’s formula and probability flow ODE based approaches for estimation the mean of the denoising distribution $\mathbb{E}_{0|t}[\mathbf{m}(0) | \mathbf{m}(t)]$.

In the Tweedie’s formula based approach, the estimated of the predicted mean, denoted $\mathbf{m}_{\text{tweedie}}$, is computed using the pretrained score model as

$$\mathbf{m}_{\text{tweedie}} = \mathbf{m}(t) + [\sigma^2(t) - \sigma^2(0)]s_{\theta^*}(\mathbf{m}(t), t). \quad (11)$$

Since the conditional distribution of $\mathbf{m}(t)$ given $\mathbf{m}(0)$ is Gaussian, Tweedie’s formula is exact and

$$\begin{aligned} \mathbb{E}_{0|t}[\mathbf{m}(0) | \mathbf{m}(t)] &= \mathbf{m}(t) \\ &+ [\sigma^2(t) - \sigma^2(0)]\nabla_{\mathbf{m}(t)} \log \pi_t(\mathbf{m}(t)). \end{aligned}$$

The only source of error in (11) is therefore score modeling error.

In the probability flow ODE based approach, the estimated mean is obtained by solving the probability flow ODE (Eq. (5)) backwards in time. For concreteness, here we consider the performance of the approach when using the backward Euler method to solve the ODE, which is commonly used in the literature [10], [16], [33].

In particular, we first consider the case with only a single reverse Euler step. In this setting, the estimate of the predicted mean, denoted \mathbf{m}_{ode} , is given by

$$\mathbf{m}_{\text{ode}} = \mathbf{m}(t) + t\sigma(t)\dot{\sigma}(t)s_{\theta^*}(\mathbf{m}(t), t). \quad (12)$$

As can be seen, the ODE and Tweedie’s formula based approaches both update $\mathbf{m}(t)$ in the direction of $s_{\theta^*}(\mathbf{m}(t), t)$. However, the magnitude of the update differs by a factor of $d = t\sigma(t)\dot{\sigma}(t)/(\sigma^2(t) - \sigma^2(0))$, which in general will not be equal to one, and so therefore $\mathbf{m}_{\text{ode}} \neq \mathbf{m}_{\text{tweedie}}$. However, under the particular choice of parameterization $\sigma(t) = t$, then $d \approx 1$ and the updates approximately coincide.

Let us now consider the same diffusion model parameterization, i.e., $\sigma(t) = t$, but with two steps used in the reverse Euler discretization. Then we have that

$$\mathbf{m}_{\text{ode}} = \mathbf{m}(t_m) + t_m^2 s_{\theta^*}(\mathbf{m}(t_m), t_m),$$

with

$$\mathbf{m}(t_m) = \mathbf{m}(t) + t(t - t_m)s_{\theta^*}(\mathbf{m}(t_m), t_m),$$

where $t_m \in (0, t)$ is the discretization point. Combining the two equations above, we have that

$$\begin{aligned} \mathbf{m}_{\text{ode}} &= \mathbf{m}(t) + t(t - t_m)s_{\theta^*}(\mathbf{m}(t_m), t_m) \\ &+ t_m^2 s_{\theta^*}(\mathbf{m}(t) + t(t - t_m)s_{\theta^*}(\mathbf{m}(t_m), t_m), t_m), \end{aligned}$$

and it is clear that in this setting, $\mathbf{m}_{\text{ode}} \neq \mathbf{m}_{\text{tweedie}}$.

The above analysis shows that the estimate of the mean of the denoising distribution given by the Tweedie’s formula based approach is exact up to error in the score model. Under a particular choice of parameterization and discretization, the probability flow ODE based approach can be made to coincide with the Tweedie’s formula based approach. However, in general the probability flow ODE based approach will introduce additional sources of error in the mean estimate that are not present in the Tweedie’s formula based approach.

ACKNOWLEDGMENTS

The authors would like to thank Dr. Sebastian Reich, Dr. Lars Ruthotto, and Dr. Nick Alger for inspiring discussions on diffusion modeling and randomize-then-optimize algorithms.

REFERENCES

- [1] J. Kaipio and E. Somersalo, *Statistical and Computational Inverse Problems*, vol. 160. Springer Science & Business Media, 2006.
- [2] A. M. Stuart, “Inverse problems: A Bayesian perspective,” *Acta Numer.*, vol. 19, pp. 451–559, 2010.
- [3] J. L. Prince and J. M. Links, *Medical Imaging Signals and Systems*. Pearson Prentice Hall Upper Saddle River, 2 ed., 2015.
- [4] R. Slingerland and L. Kump, *Mathematical modeling of Earth’s dynamical systems: A primer*. Princeton University Press, 2011.
- [5] S. Chan *et al.*, “Tutorial on diffusion models for imaging and vision,” *Foundations and Trends® in Computer Graphics and Vision*, vol. 16, no. 4, pp. 322–471, 2024.

- [6] L. Ruthotto and E. Haber, “An introduction to deep generative modeling,” *GAMM-Mitteilungen*, vol. 44, no. 2, p. e202100008, 2021.
- [7] A. Bora, A. Jalal, E. Price, and A. G. Dimakis, “Compressed sensing using generative models,” in *Proc. Int. Conf. Mach. Learn.*, pp. 537–546, PMLR, 2017.
- [8] Y. Song and S. Ermon, “Generative modeling by estimating gradients of the data distribution,” in *Adv. Neural Inf. Process. Syst.*, vol. 32, 2019.
- [9] J. Ho, A. Jain, and P. Abbeel, “Denoising diffusion probabilistic models,” in *Adv. Neural Inf. Process. Syst.*, vol. 33, pp. 6840–6851, 2020.
- [10] Y. Song, J. Sohl-Dickstein, D. P. Kingma, A. Kumar, S. Ermon, and B. Poole, “Score-based generative modeling through stochastic differential equations,” in *Proc. Int. Conf. Learn. Represent.*, 2021.
- [11] A. Jalal, M. Arvinte, G. Daras, E. Price, A. G. Dimakis, and J. Tamir, “Robust compressed sensing MRI with deep generative priors,” in *Adv. Neural Inf. Process. Syst.*, vol. 34, pp. 14938–14954, 2021.
- [12] Y. Song, L. Shen, L. Xing, and S. Ermon, “Solving inverse problems in medical imaging with score-based generative models,” in *Proc. Int. Conf. Learn. Represent.*, 2022.
- [13] H. Chung, B. Sim, D. Ryu, and J. C. Ye, “Improving diffusion models for inverse problems using manifold constraints,” in *Adv. Neural Inf. Process. Syst.*, vol. 35, pp. 25683–25696, Curran Associates, Inc., 2022.
- [14] H. Chung, J. Kim, M. T. McCann, M. L. Klasky, and J. C. Ye, “Diffusion posterior sampling for general noisy inverse problems,” in *Proc. Int. Conf. Learn. Represent.*, 2023.
- [15] Z. Wu, Y. Sun, Y. Chen, B. Zhang, Y. Yue, and K. L. Bouman, “Principled probabilistic imaging using diffusion models as plug-and-play priors,” in *Adv. Neural Inf. Process. Syst.*, 2024.
- [16] B. Zhang, W. Chu, J. Berner, C. Meng, A. Anandkumar, and Y. Song, “Improving diffusion inverse problem solving with decoupled noise annealing,” *arXiv preprint arXiv:2407.01521*, 2024.
- [17] Y. Zhu, K. Zhang, J. Liang, J. Cao, B. Wen, R. Timofte, and L. Van Gool, “Denoising diffusion models for plug-and-play image restoration,” in *Proc. Conf. Comput. Vis. Pattern Recognit.*, pp. 1219–1229, 2023.
- [18] J. M. Bardsley, A. Solonen, H. Haario, and M. Laine, “Randomize-then-optimize: A method for sampling from posterior distributions in nonlinear inverse problems,” *SIAM J. Sci. Comput.*, vol. 36, no. 4, pp. A1895–A1910, 2014.
- [19] K. Wang, T. Bui-Thanh, and O. Ghattas, “A randomized maximum a posteriori method for posterior sampling of high dimensional nonlinear bayesian inverse problems,” *SIAM J. Sci. Comput.*, vol. 40, no. 1, pp. A142–A171, 2018.
- [20] W. Zellinger, T. Grubinger, E. Lughofer, T. Natschläger, and S. Saminger-Platz, “Central moment discrepancy (CMD) for domain-invariant representation learning,” in *Proc. Int. Conf. Learn. Represent.*, 2017.
- [21] A. Gretton, K. M. Borgwardt, M. J. Rasch, B. Schölkopf, and A. Smola, “A kernel two-sample test,” *J. Mach. Learn. Res.*, vol. 13, no. 1, pp. 723–773, 2012.
- [22] B. D. Anderson, “Reverse-time diffusion equation models,” *Stoch. Process. Their Appl.*, vol. 12, no. 3, pp. 313–326, 1982.
- [23] C. Lu, K. Zheng, F. Bao, J. Chen, C. Li, and J. Zhu, “Maximum likelihood training for score-based diffusion odes by high order denoising score matching,” in *Proc. Int. Conf. Mach. Learn.*, pp. 14429–14460, 2022.
- [24] Y. Song, C. Durkan, I. Murray, and S. Ermon, “Maximum likelihood training of score-based diffusion models,” *Adv. Neural Inf. Process. Syst.*, vol. 34, pp. 1415–1428, 2021.
- [25] P. Vincent, “A connection between score matching and denoising autoencoders,” *Neural Comput.*, vol. 23, no. 7, pp. 1661–1674, 2011.
- [26] B. Boys, M. Girolami, J. Pidstrigach, S. Reich, A. Mosca, and O. D. Akyildiz, “Tweedie moment projected diffusions for inverse problems,” *Trans. Mach. Learn. Res.*, 2024.
- [27] J. Song, A. Vahdat, M. Mardani, and J. Kautz, “Pseudoinverse-guided diffusion models for inverse problems,” in *Proc. Int. Conf. Learn. Represent.*, 2023.
- [28] J. Yu, Y. Wang, C. Zhao, B. Ghanem, and J. Zhang, “FreeDoM: Training-free energy-guided conditional diffusion model,” in *Proc. IEEE Int. Conf. Comput. Vis.*, pp. 23174–23184, 2023.
- [29] B. Efron, “Tweedie’s formula and selection bias,” *J. Am. Stat. Assoc.*, vol. 106, no. 496, pp. 1602–1614, 2011.
- [30] C. Meng, Y. Song, W. Li, and S. Ermon, “Estimating high order gradients of the data distribution by denoising,” in *Adv. Neural Inf. Process. Syst.*, vol. 34, pp. 25359–25369, 2021.
- [31] S. H. Chan, X. Wang, and O. A. Elgandy, “Plug-and-play ADMM for image restoration: Fixed-point convergence and applications,” *IEEE Trans. Comput. Imaging*, vol. 3, no. 1, pp. 84–98, 2016.
- [32] N. Parikh and S. Boyd, *Proximal Algorithms*, vol. 1 of *Foundations and Trends® in Optimization*. Now Publishers, Inc., 2013.
- [33] J. Song, C. Meng, and S. Ermon, “Denoising diffusion implicit models,” in *Proc. Int. Conf. Learn. Represent.*, 2021.
- [34] I. Alkhouri, S. Liang, C.-H. Huang, J. Dai, Q. Qu, S. Ravishanker, and R. Wang, “Sitcom: Step-wise triple-consistent diffusion sampling for inverse problems,” *arXiv preprint arXiv:2410.04479*, 2024.
- [35] B. Song, S. M. Kwon, Z. Zhang, X. Hu, Q. Qu, and L. Shen, “Solving inverse problems with latent diffusion models via hard data consistency,” *arXiv preprint arXiv:2307.08123*, 2023.
- [36] R. M. Neal, “MCMC using Hamiltonian dynamics,” in *Handbook of Markov Chain Monte Carlo* (S. Brooks, A. Gelman, G. L. Jones, and X.-L. Meng, eds.), ch. 5, pp. 113–162, Chapman & Hall/CRC, 2011.
- [37] Y. Ba, J. de Wiljes, D. S. Oliver, and S. Reich, “Randomized maximum likelihood based posterior sampling,” *Comput. Geosci.*, vol. 26, no. 1, pp. 217–239, 2022.
- [38] J. M. Bardsley, “MCMC-based image reconstruction with uncertainty quantification,” *SIAM J. Sci. Comput.*, vol. 34, no. 3, pp. A1316–A1332, 2012.
- [39] T. Ge, U. Villa, U. S. Kamilov, and J. A. O’Sullivan, “Proximal Newton methods for X-Ray imaging with non-smooth regularization,” *J. Electron. Imaging*, vol. 32, no. 14, pp. 7–1–7–1, 2020.
- [40] Y. Shechtman, Y. C. Eldar, O. Cohen, H. N. Chapman, J. Miao, and M. Segev, “Phase retrieval with application to optical imaging: A contemporary overview,” *IEEE Signal Process. Mag.*, vol. 32, no. 3, pp. 87–109, 2015.
- [41] M. Girolami and B. Calderhead, “Riemann manifold Langevin and Hamiltonian Monte Carlo methods,” *J. R. Stat. Soc.*, vol. 73, no. 2, pp. 123–214, 2011.
- [42] J. Nocedal and S. J. Wright, *Numerical optimization*. Springer, 1999.
- [43] D. P. Kingma and J. Ba, “Adam: A method for stochastic optimization,” *arXiv preprint arXiv:1412.6980*, 2014.
- [44] E. M. Shockley, J. A. Vrugt, and C. F. Lopez, “PyDREAM: High-dimensional parameter inference for biological models in Python,” *Bioinformatics*, vol. 34, no. 4, pp. 695–697, 2018.
- [45] E. Laloy and J. A. Vrugt, “High-dimensional posterior exploration of hydrologic models using multiple-try DREAM (ZS) and high-performance computing,” *Water Resour. Res.*, vol. 48, no. 1, 2012.
- [46] W.-L. Loh, “On Latin hypercube sampling,” *Ann. Stat.*, vol. 24, no. 5, pp. 2058–2080, 1996.
- [47] T. O’Leary-Roseberry, P. Chen, U. Villa, and O. Ghattas, “Derivative-informed neural operator: An efficient framework for high-dimensional parametric derivative learning,” *J. Comput. Phys.*, vol. 496, p. 112555, 2024.

Supplementary Material For “Can Diffusion Models Provide Rigorous Uncertainty Quantification for Bayesian Inverse Problems?”

Evan Scope Crafts¹, Member, IEEE, and Umberto Villa¹, Member, IEEE

¹Oden Institute for Computational Engineering and Sciences, The University of Texas at Austin, Austin, TX USA 78712

In this document, we provide additional analysis of the results of the numerical studies. In particular, we use violin plots [1] of the central moment discrepancy (CMD) and maximum mean discrepancy (MMD) errors to provide additional insight into how the BIPSDA algorithms perform across the posterior sampling trials. The ground-truth and BIPDA algorithm posterior samples for all four studies are also provided at: <https://doi.org/10.7910/DVN/0L5KGB> to facilitate further analysis of the data.

Figure S1 shows two-sided violin plots of the CMD and MMD errors across posterior sampling trials for the stylized inpainting study in the low noise regime. Note that in these violin plots, and all subsequent violin plots, the densities have been normalized to have unit width for ease of visualization. As can be seen, the learned score model is not a major source of error in the posterior sampling. Further, while all BIPSDA algorithms perform well on this problem, the Lang-ODE, RTO-TU, and RTO-TC (with analytic score) achieve the strongest performance of the algorithms we tested.

Figure S2 shows the corresponding plots in the high noise regime. As can be seen, the Langevin-based approaches perform poorly across the trials. The RTO-based approaches perform well with respect to both the CMD and MMD metrics, but have high variance across the trials—there is a two-order-of-magnitude difference in performance between the best-performing and worst-performing trials. The MAP based approaches are competitive with the RTO based approaches with respect to the CMD metric but perform significantly worse with respect to the MMD metric. This is not a surprising result, as the MAP based approaches underestimate the variance of the posterior modes and the MMD metric is very sensitive to the local structure of the distributions.

Figure S3 displays the violin plots corresponding to the stylized x-ray tomography study. As can be seen, while all approaches we tested perform competitively on this problem, the RTO-TU and RTO-TC (with analytic score) approaches perform the best across the trials and are capable of achieving very high accuracy. We also note that RTO-ODE approach performs significantly worse than the RTO-TU and RTO-TC approaches. This result, which is consistent with observations in the other three studies we conducted, suggests that the TU and TC techniques are better suited for use with the RTO sampler in our framework.

Figure S4 shows the violin plots for the phase retrieval study. As can be seen, the performance of all of the BIPSDA algorithms we tested varies significantly across the trials. While the algorithms are all capable of achieving strong performance on some of the trials, they also all struggle to perform well on the more difficult trials. Specifically, the algorithms struggle to perform well when the posterior is multi-modal and the modes are highly separated. Additional work is therefore required to achieve strong performance on this challenging problem.

REFERENCES

[1] J. L. Hintze and R. D. Nelson, “Violin plots: A box plot-density trace synergism,” *Am. Stat.*, vol. 52, no. 2, pp. 181–184, 1998.

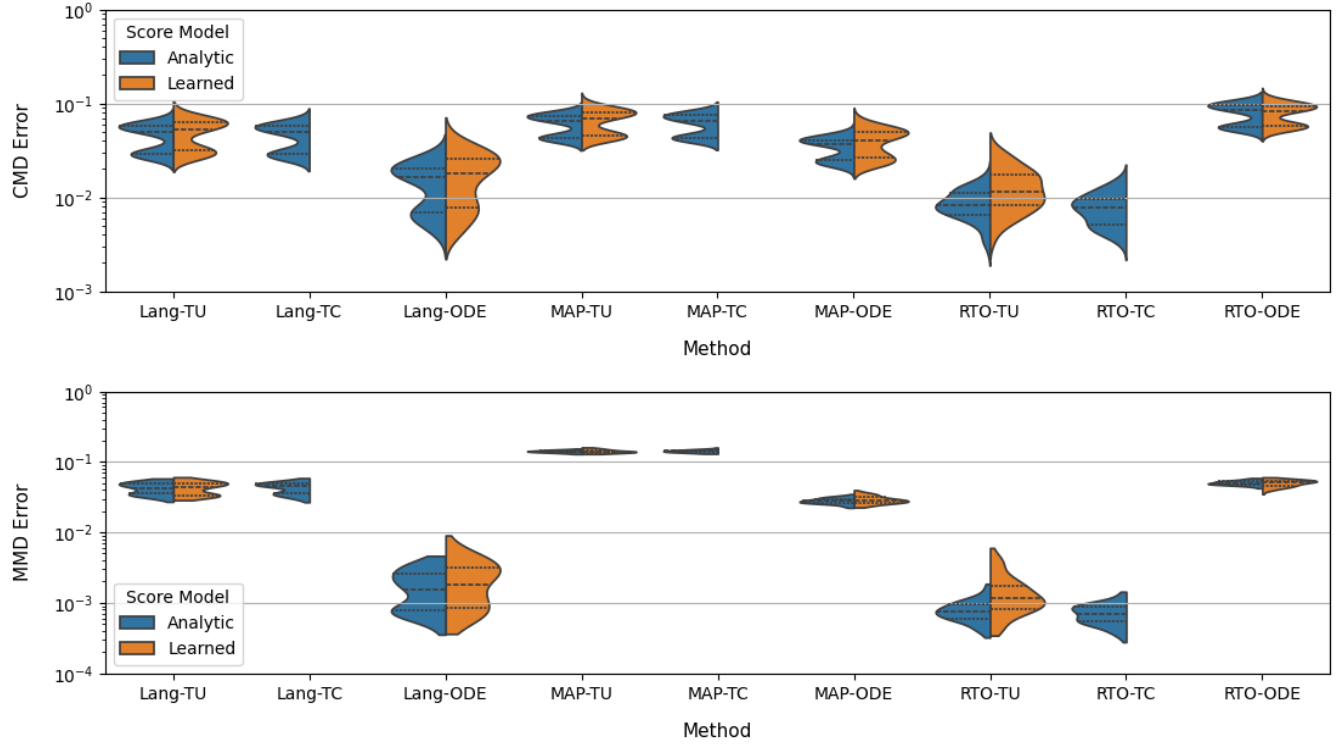


FIGURE S1. Stylized inpainting study, low noise regime: Two-sided violin plots of the CMD errors (top) and MMD errors (bottom) across the one hundred trials. Note that the violin kernel densities in this and all subsequent plots were normalized to have unit width for ease of visualization. As can be seen, the Lang-ODE, RTO-TU, and RTO-TC (in analytic score setting) approaches are the best performing with respect to both the CMD and MMD metrics.

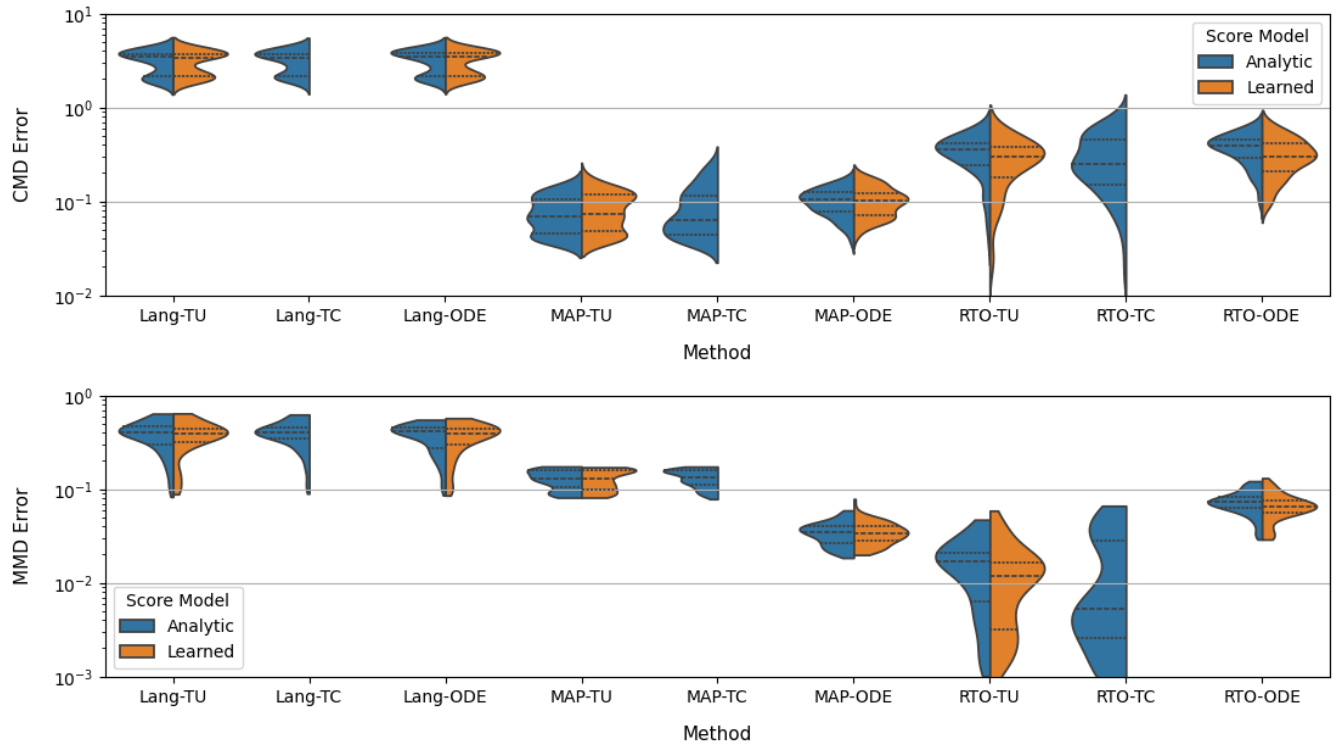


FIGURE S2. Stylized inpainting study, high noise regime: Two-sided violin plots of the CMD errors (top) and MMD errors (bottom) across the one hundred trials. As can be seen, the Langevin dynamics based approaches perform poorly in this problem setting.

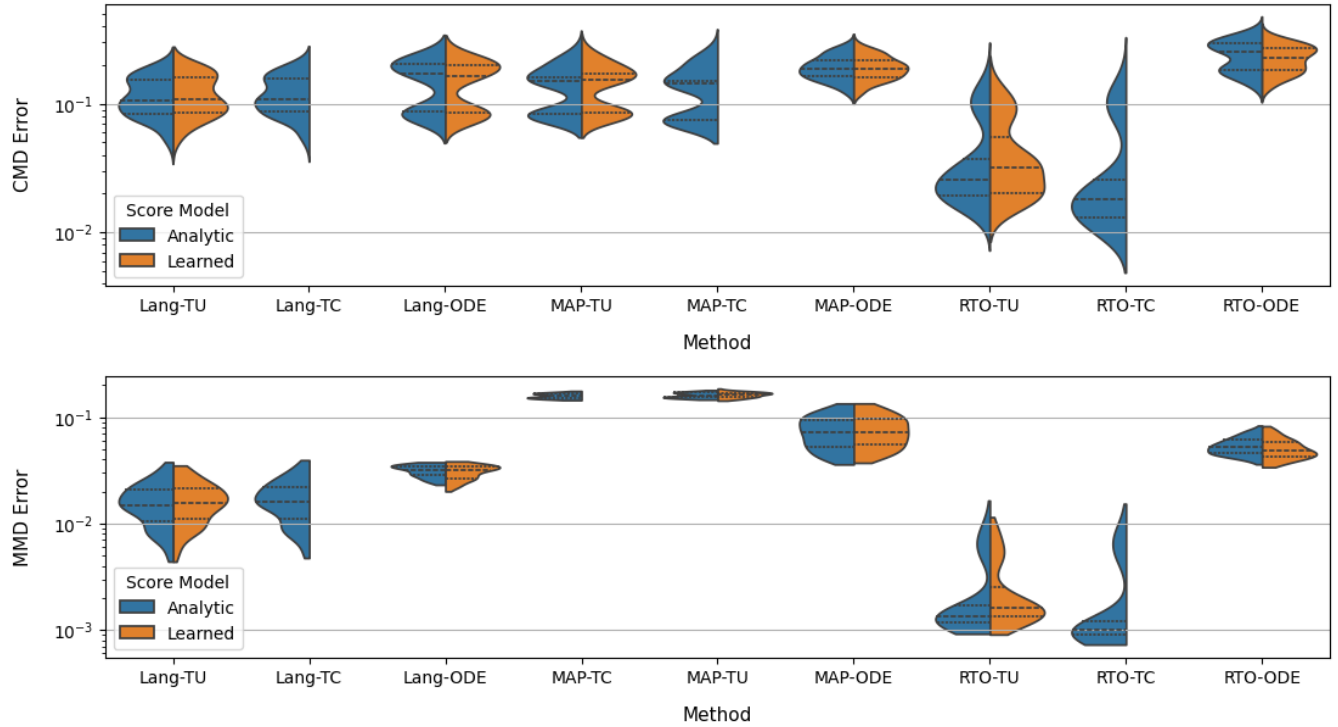


FIGURE S3. Stylized x-ray tomography study: Two-sided violin plots of the CMD errors (top) and MMD errors (bottom) across the one hundred trials. As can be seen, the RTO-TU and RTO-TC (in analytic score setting) approaches achieve the best performance of the algorithms tested with respect to both metrics.

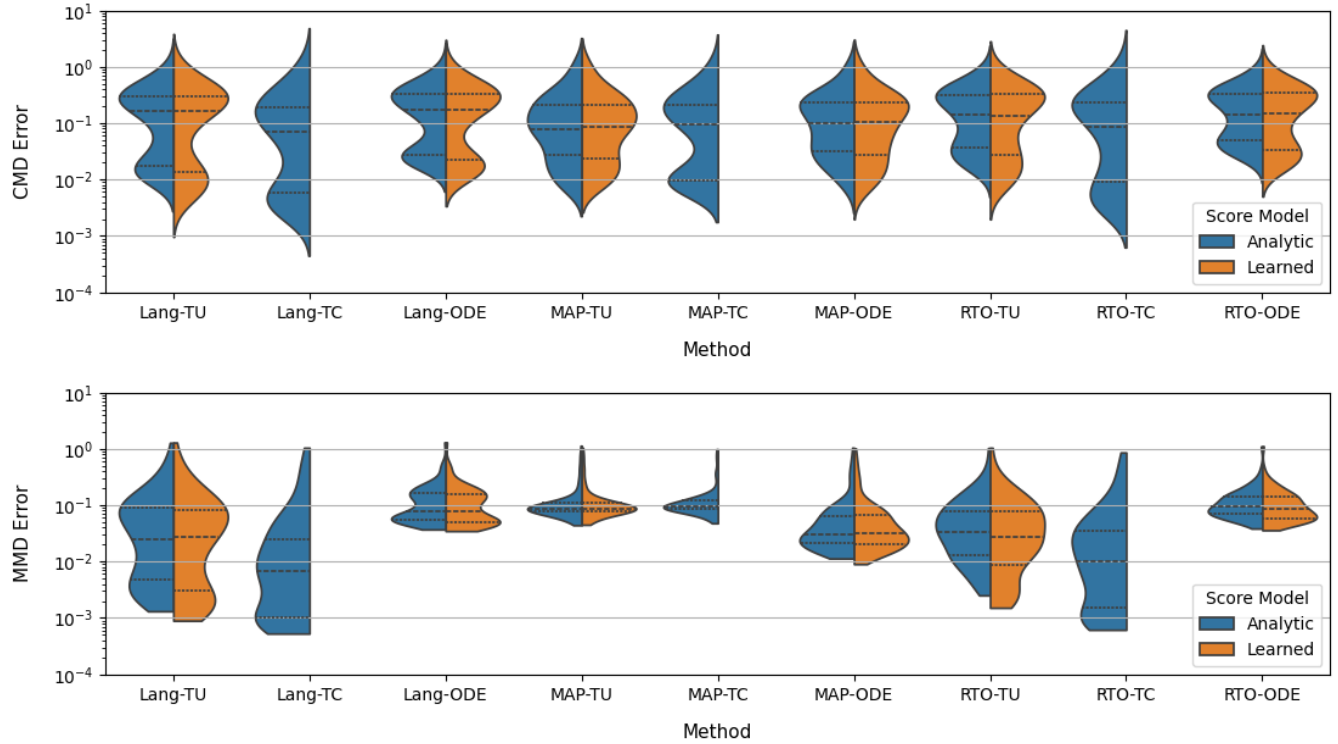


FIGURE S4. Stylized phase retrieval study: Two-sided violin plots of the CMD errors (top) and MMD errors (bottom) across the one hundred trials. As can be seen, the performance of all of the BIPSDA algorithms we tested varies significantly across the trials, with none of the algorithms providing consistently strong performance.